

Universal Architectures for the Learning of Polyhedral Norms and Convex Regularization Functionals*

Michael Unser and Stanislas Ducotterd[†]

March 26, 2025

Abstract

This paper addresses the task of learning convex regularizers to guide the reconstruction of images from limited data. By imposing that the reconstruction be amplitude-equivariant, we narrow down the class of admissible functionals to those that can be expressed as a power of a seminorm. We then show that such functionals can be approximated to arbitrary precision with the help of polyhedral norms. In particular, we identify two dual parameterizations of such systems: (i) a synthesis form with an ℓ_1 -penalty that involves some learnable dictionary; and (ii) an analysis form with an ℓ_∞ -penalty that involves a trainable regularization operator. After having provided geometric insights and proved that the two forms are universal, we propose an implementation that relies on a specific architecture (tight frame with a weighted ℓ_1 penalty) that is easy to train. We illustrate its use for denoising and the reconstruction of biomedical images. We find that the proposed framework outperforms the sparsity-based methods of compressed sensing, while it offers essentially the same convergence and robustness guarantees.

*The research leading to these results has received funding from the European Research Council under Grant ERC-2020-AdG FunLearn-101020573.

[†]Biomedical Imaging Group, École polytechnique fédérale de Lausanne (EPFL), Station 17, CH-1015, Lausanne, Switzerland (michael.unser@epfl.ch).

Contents

1	Introduction	2
2	Problem Formulation	5
2.1	Variational Setup for the Resolution of Inverse Problems . . .	5
2.2	Equivariant Regularizers	5
3	Universal Equivariant Convex Regularizers	8
3.1	Properties of the Unit Regularization Ball	9
3.2	Universal Parametric Polyhedral Regularizers	10
4	Supporting Banach-Space Theory	14
4.1	Nomenclature and notation	14
4.2	Polyhedral Banach Spaces	15
5	Parametric Reconstruction Pipelines	20
5.1	Sparse Encoding in a Frame/Dictionary	20
5.2	Universal Weighted ℓ_∞ -Regularization	21
5.3	Weighted ℓ_1 -Regularization Revisited	22
5.4	Implementation of a Trainable Convex Regularizer	23
5.5	Experimental results	25
5.5.1	Training	26
5.5.2	Denoising results	27
5.5.3	MRI Reconstruction	27
5.6	Discussion	29
	Appendix A: (Semi)norms and Banach Duality	30

1 Introduction

The context of this work is computational imaging where the goal is to reconstruct an image from indirect and possibly incomplete measurements. We focus on scenarios where the measurements are linear functionals of the object under investigation, such as line integrals in computer tomography [1] or samples of its Fourier transform in magnetic resonance imaging [2]. These quantities are corrupted by noise according to the relation $\mathbf{y} = \mathbf{H}\mathbf{s} + \mathbf{n}_{\text{noise}} \in \mathbb{R}^M$, where $\mathbf{s} \in \mathbb{R}^d$ is the unknown signal to be recovered and $\mathbf{H} \in \mathbb{R}^{M \times d}$ is the system matrix that results from the discretization of the physics.

Given a candidate signal $\tilde{\mathbf{s}}$, the forward model is simulated as $\mathbf{H}\tilde{\mathbf{s}}$ which, for consistency, ought to match \mathbf{y} within the noise level.

Computational imaging is currently dominated by two paradigms [3]. The first one is the variational approach, where the reconstruction task is formulated as a cost minimization problem, as in (1). Variational techniques have driven the development of image reconstruction algorithms over the past three decades. They are supported by an extensive theory and benefit from the powerful computational tools of convex optimization [4, 5] and compressed sensing [6]. Solutions are typically computed iteratively through the minimization a cost, either by steepest descent or by proximal-gradient techniques [7, 8, 9, 10]. Under standard hypotheses (convexity and coercivity of the cost functional), this framework provides guarantees for convergence [4], stability [11], and signal recovery from limited measurements [12, 13].

The second paradigm, at the forefront of research, is the data-driven approach, often referred to as artificial intelligence (AI), where the traditional reconstruction pipeline is replaced or complemented by deep neural networks (DNN) [14, 15, 16, 17]. Formally, the resulting reconstruction algorithm is a nonlinear map $\mathbf{f}_\theta : \mathbb{R}^M \rightarrow \mathbb{R}^d$ with parameters θ (the weights of the neural net). These are pre-trained for best performance in a regression task such that $\mathbf{f}_\theta(\mathbf{y}_k) \approx \mathbf{x}_k$ on a representative set of data $(\mathbf{s}_k, \mathbf{y}_k)_{k=1}^K$, where K (the number of training images) is assumed to be sufficiently large. DNN-based methods generally achieve superior image reconstructions [18] but suffer from a lack of robustness [19] and theoretical understanding. More importantly, they have been found to remove or hallucinate structures [20, 21], which is unacceptable in medical imaging.

Hybrid approaches aim to combine the strengths of both paradigms, typically by learning the regularization functional $g = g_\theta$ in (1) [22, 23], or by unrolling the corresponding iterative algorithm into a trainable architecture [24]. One of the earliest hybrid approach is the field of expert (FoE) model [25], where the regularization functional $g(\mathbf{s}) = \sum_k \phi_k(\mathbf{w}_k^\top \mathbf{s}) = \langle \mathbf{1}, \Phi(\mathbf{W}\mathbf{s}) \rangle$ is a sum of ridges. These ridges result from the application of a convex function $\phi_k : \mathbb{R} \rightarrow \mathbb{R}^+$ (potential) to some filtered versions of the signal, with the filtering templates \mathbf{w}_k (collectively encoded in \mathbf{W}) being learned. Variants of this strategy include schemes where the potentials themselves are trainable under a convexity constraint [26, 27, 28]. Another prominent strategy is the plug-and-play (PnP) framework [29, 30], where deep-learning-based denoisers replace traditional proximal operators [31, 32, 33]. For these methods to remain variational, the learned denoiser must satisfy both firm non-expansiveness (for convergence [34, Proposition 15]) and monotonicity [35, 36], the latter being challenging to enforce.

This raises a fundamental question: To what extent can one improve variational methods by learning the regularizer, while maintaining their theoretical guarantees? While the FoE model substantially improves upon “hand-crafted” regularizers such as total variation (TV) [37], its expressiveness may still be insufficient to capture the full range of convex regularizations. We contend that further improvements are possible within the variational framework under adequate constraints to avoid hallucinations.

To address these issues, we introduce a general parametric framework for image reconstruction under the constraints of amplitude equivariance (AE) and convexity. This parameterization involves polyhedral norms and results in a formulation that is reminiscent of compressed-sensing techniques with a trainable dictionary [38, 39]. Our present contribution is two fold:

1. The identification of two dual forms of polyhedral regularization with proof of their universality, in the sense that they are able to encode any AE convex regularizer to an ϵ -level of precision.
2. The transcription of the theory into practical reconstruction architectures, including a constrained version that lends itself well to training.

The paper is organized as follows. In Section 2, we formalize the variational reconstruction problem and invoke higher-level principles (amplitude-equivariance and coercivity) to narrow down the class of admissible regularization functionals to some power of a norm, as dictated by Theorem 1. In Section 3, we prove that we can achieve universality with the help of polyhedral norms (Theorem 4), the latter admitting two dual parameterizations in terms of some linear operator, as stated in Theorem 3. The theoretical foundation for our results is presented in Section 4 with a complete characterization of the geometry of polyhedral Banach spaces (Theorem 5). In Section 5, we use our results to specify explicit computational architectures, including one that relies on weighted ℓ_1 -minimization and Parseval filterbanks, which is easy to train. We then demonstrate that this approach provides competitive results for denoising and image reconstruction.

2 Problem Formulation

2.1 Variational Setup for the Resolution of Inverse Problems

Given the data $\mathbf{y} \in \mathbb{R}^M$ and a linear measurement model, the generic variational formulation of our signal-reconstruction problem is

$$\min_{\mathbf{s} \in \mathbb{R}^d} \left(\frac{1}{2} \|\mathbf{y} - \mathbf{H}\mathbf{s}\|_2^2 + \lambda g(\mathbf{s}) \right), \quad (1)$$

where $\mathbf{H} \in \mathbb{R}^{M \times d}$ is a known matrix that models the physics of the acquisition, and where $g : \mathbb{R}^d \rightarrow \mathbb{R}^+$ is a regularization functional that promotes “regular” solutions. The relative strength of the regularization is modulated by the regularization factor $\lambda \in \mathbb{R}^+$, according to the standard practice in the field. In this work, we aim at investigating schemes where $g = g_{\boldsymbol{\theta}}$ is a learned regularizer with trainable parameters collected in $\boldsymbol{\theta}$.

Since our goal is to identify useful classes of regularizers, we can focus on the noise-free scenario (the limit case of (1) as $\lambda \rightarrow 0$), without loss of generality. The solution of the corresponding generalized interpolation problem reads

$$\mathbf{f}_{\boldsymbol{\theta}}(\mathbf{y}) = \arg \min_{\mathbf{s} \in \mathbb{R}^d} \{g_{\boldsymbol{\theta}}(\mathbf{s}) \text{ s.t. } \mathbf{y} = \mathbf{H}\mathbf{s}\}, \quad (2)$$

where $\mathbf{f}_{\boldsymbol{\theta}} : \mathbb{R}^M \rightarrow \mathbb{R}^d$ denotes the underlying (nonlinear) reconstruction operator that implements the minimization and depends on the hyperparameters $\boldsymbol{\theta}$ of the regularization functional $g_{\boldsymbol{\theta}}$. The underlying assumption here is that (2) with $\boldsymbol{\theta}$ fixed is well-defined with a unique global minimum.

2.2 Equivariant Regularizers

Since the measurement operator in (1) is linear, a change of amplitude of the signal \mathbf{s} by the multiplicative factor α results in a corresponding rescaling of the measurements, as in $\alpha\mathbf{y} = \mathbf{H}(\alpha\mathbf{s})$. Accordingly, we shall insist that this property also carry over to the reconstruction specified by (2) in the noise-free scenario and, more generally, by (1) for λ sufficiently small, say, below some critical value $\lambda_0 = \lambda(\mathbf{y})$. Specifically, when we amplify the measurements and signal by the same factor $\alpha \neq 0$, we get that

$$\arg \min_{\mathbf{s} \in \mathbb{R}^d} \frac{1}{2} \|\alpha\mathbf{y} - \mathbf{H}\alpha\mathbf{s}\|_2^2 + \lambda_0 g_{\boldsymbol{\theta}}(\alpha\mathbf{s}) = \arg \min_{\mathbf{s} \in \mathbb{R}^d} \frac{1}{2} \|\mathbf{y} - \mathbf{H}\mathbf{s}\|_2^2 + \frac{\lambda_0}{\alpha^2} g_{\boldsymbol{\theta}}(\alpha\mathbf{s}),$$

which, according to our requirement, needs to remain compatible with (1). The desired equivalence is achieved for $\lambda = \frac{\lambda_0}{\alpha^2} \frac{g_{\boldsymbol{\theta}}(\alpha\mathbf{s})}{g_{\boldsymbol{\theta}}(\mathbf{s})}$, but only under the

condition that the ratio does not depend upon \mathbf{s} . This is to say that the effect of scaling needs to factor out of the regularization, which is a property that we shall refer to as *amplitude equivariance*.

Definition 1. *A regularization functional $g : \mathcal{X} \rightarrow \mathbb{R}$ is said to be amplitude-equivariant if there exists a function $a : \mathbb{R} \rightarrow \mathbb{R}$ such that $g(\alpha x) = a(\alpha)g(x)$ for any $x \in \mathcal{X}$ and $\alpha \in \mathbb{R} \setminus \{0\}$.*

By adding conditions of convexity to ensure that the solution of (1) or that of (2) exist along with symmetry (which is standard in image processing), we now show that we can narrow down the options to $g(\mathbf{x}) = |p(\mathbf{x})|^\gamma$, where p is a seminorm on $\mathcal{X} = \mathbb{R}^d$ and $\gamma \geq 1$.

To state our result, we first single out some relevant properties.

Definition 2. *Let $g : \mathcal{X} \rightarrow \mathbb{R}$ be a (regularization) functional on a Banach space \mathcal{X} . Then, f can be endowed with the following properties.*

1. *Unbiasedness: $g(x) \geq g(0)$ for all $x \in \mathcal{X}$.*
2. *Symmetry: $g(x) = g(-x)$ for all $x \in \mathcal{X}$.*
3. *Convexity: $g(\lambda x + (1 - \lambda)y) \leq \lambda g(x) + (1 - \lambda)g(y)$ for all $x, y \in \mathcal{X}$ and $\lambda \in [0, 1]$.*
4. *Homogeneity: $g(\alpha x) = |\alpha|g(x)$ for all $x \in \mathcal{X}$ and $\alpha \in \mathbb{R} \setminus \{0\}$.*
5. *Homogeneity of order γ : $g(\alpha x) = |\alpha|^\gamma g(x)$ for all $x \in \mathcal{X}$, $\alpha \in \mathbb{R} \setminus \{0\}$ and $\gamma \in \mathbb{R}_{>0}$.*

Theorem 1. *Let $g : \mathcal{X} \rightarrow \mathbb{R}$ be a convex, symmetric (and continuous) functional on the Banach space \mathcal{X} . Then, the following equivalences hold.*

1. *The functional g is γ -homogeneous for some $\gamma \geq 1$ if and only if it is amplitude-equivariant.*
2. *It is amplitude-equivariant if and only if $g(x) = |p(x)|^\gamma$, where p is a seminorm and γ the order of homogeneity of g .*

The reason why “continuity” is parenthesized in the statement of Theorem 1 is that the hypothesis is superfluous in the finite-dimensional setting because: (i) all Banach norms, as well as the associated notions of continuity, are equivalent on \mathbb{R}^d [40]; and (ii) all convex functions $g : \mathbb{R}^d \rightarrow \mathbb{R}$ are continuous on their domain [4, 5]. We also note that the covered scenarios all require that g be symmetric and unbiased with $g(0) = 0$.

Proof. First, we observe that γ th-order homogeneity (with $\alpha = -1$) implies symmetry. The statements in the theorem summarize the following chain of implications, with the first three items covering the classic equivalence: convex homogeneous functional = seminorm (see Appendix A, Definition 6).

1. Convexity + homogeneity \Rightarrow subadditivity. It suffices to take the convexity inequality with $\lambda = \frac{1}{2}$.
2. Subadditivity + homogeneity \Rightarrow convexity: $g(\lambda x + (1 - \lambda)y) \leq g(\lambda x) + g((1 - \lambda)y) = \lambda g(x) + (1 - \lambda)g(y)$.
3. Subadditivity + symmetry $\Rightarrow g(x) \geq g(0) = 0$ for all $x \in \mathcal{X}$: Subadditivity with $x = 0$ gives $g(y) \leq g(0) + g(y)$, which implies that $g(0) = 0$. Likewise, for $y = -x$, we get that $g(0) = g(x - x) \leq g(x) + g(-x) = 2g(x)$ for all $x \in \mathcal{X}$.
4. Convexity + symmetry $\Rightarrow g(x) \geq g(0)$ for all $x \in \mathcal{X}$: Indeed, $g(0) = g(\frac{1}{2}x + \frac{1}{2}(-x)) \leq \frac{1}{2}g(x) + \frac{1}{2}g(-x) = g(x)$.
5. Convexity and γ th-order homogeneity $\Rightarrow \gamma \geq 1$: For any $\alpha \leq (0, 1)$ and $x \in \mathcal{X}$, we must have that $g(\alpha x + 0) = (\alpha)^\gamma g(x) \leq \alpha g(x)$, which implies that $\gamma \geq 1$.
6. Continuity and γ th-order homogeneity $\Rightarrow g(0) = 0$: Given some arbitrary $x_0 \in \mathcal{X} \setminus \{0\}$, we construct the sequence $x_n = \frac{1}{n}x_0 \neq 0$. It is converging to 0 in \mathcal{X} because $\|x_n\|_{\mathcal{X}} = \frac{1}{n}\|x_0\|_{\mathcal{X}} \rightarrow 0$ as $n \rightarrow \infty$. By invoking the γ -homogeneity and continuity of g , we then get that

$$\lim_{n \rightarrow \infty} g(x_n) = \lim_{n \rightarrow \infty} \left(\frac{1}{n}\right)^\gamma g(x_0) = 0 = g\left(\lim_{n \rightarrow \infty} x_n\right) = g(0).$$

7. Amplitude-equivariance $\Leftrightarrow \gamma$ th-order homogeneity: Let $\alpha = \alpha_1 \alpha_2 > 0$. Then, $g(\alpha x) = a(\alpha)g(x) = a(\alpha_1)a(\alpha_2)g(x)$, which implies that

$$a(\alpha_1 \alpha_2) = a(\alpha_1)a(\alpha_2) \Leftrightarrow \log a(\alpha_1 \alpha_2) = \log a(\alpha_1) + \log a(\alpha_2).$$

This means that the function $\log a : \mathbb{R}_{>0} \rightarrow \mathbb{R}$ is linear and hence of the form $\log a(\alpha) = C_0 \alpha$, which is the desired result with $C_0 = \log \gamma$. The reverse implication is obvious.

8. Convexity and γ th-order homogeneity $\Leftrightarrow g(x) = |p(x)|^\gamma$, where p is convex and 1-homogeneous.

Indirect part: The function $g(x) = |p(x)|^\gamma$ is convex because it is the

composition of two convex functionals $p : \mathcal{X} \rightarrow \mathbb{R}_{\geq 0}$ and $|\cdot|^\gamma : \mathbb{R}_{\geq 0} \rightarrow \mathbb{R}_{\geq 0}$. Moreover, it is such that $g(x) = |p(\alpha x)|^\gamma = |\alpha p(x)|^\gamma = |\alpha|^\gamma g(x)$.

Direct part: We now show that the convexity of $g(x) \geq 0$ implies that of $p(x) = (g(x))^{1/\gamma}$, which is 1-homogeneous. For any $x, y \in \mathcal{X}$ with $p(x), p(y) \neq 0$ and $\lambda \in [0, 1]$ and by letting $P = \lambda p(x) + (1-\lambda)p(y) > 0$, we have that

$$\begin{aligned} \frac{g(\lambda x + (1-\lambda)y)}{P^\gamma} &= g\left(\frac{\lambda p(x)}{P} \frac{x}{p(x)} + \frac{(1-\lambda)p(y)}{P} \frac{x}{p(y)}\right) \\ &\leq \frac{\lambda p(x)}{P} g\left(\frac{x}{p(x)}\right) + \frac{(1-\lambda)p(y)}{P} g\left(\frac{y}{p(y)}\right) \\ &= \frac{\lambda p(x)}{P} + \frac{(1-\lambda)p(y)}{P} = 1, \end{aligned} \quad (3)$$

where we also used that $g(x) = p(x)^\gamma$. We then take the γ th root of (3), which yields the desired convexity inequality $p(\lambda x + (1-\lambda)y) \leq P$. (The latter obviously also holds for $p(x) = 0$ and/or $p(y) = 0$ because of the homogeneity of p .)

□

In the context of regularization, the amplitude-equivariance property is fundamental for it ensures that the recovery procedure is covariant (through a proper adjustment of the regularization strength) to any global rescaling of the input data. In view of Theorem 1, this reduces the options of acceptable regularizations to (semi)norms. Since $|\cdot|^\gamma$ is increasing convex, we also note that there is no loss of generality if we replace g_θ in (2) by $p = |g|^{1/\gamma}$. The same holds true for (1) under a suitable adjustment of the regularization parameter λ .

If we also want to make sure that the solution of Problem (1) exists, irrespective of the system matrix \mathbf{H} , we need p to be coercive [4], which then narrows down the options to the case where p is a norm.

3 Universal Equivariant Convex Regularizers

So far, we have seen that a coercive, equivariant convex regularizer g can always be replaced by an appropriate norm p on \mathbb{R}^d . Our next step will be to show that this can all be reformulated using convex sets. We then attain universality by approximating the underlying regularization balls as closely as desired with the help of (learned) polytopes. The crucial issue there is to retain the norm property, which is fundamental to our argumentation.

3.1 Properties of the Unit Regularization Ball

A basic result in functional analysis is that every seminorm p on a vector space \mathcal{X} has an equivalent geometric description in terms of the characteristic set: $B = B_p = \{x \in \mathcal{X} : p(x) \leq 1\}$, which happens to be a disk. The key to this equivalence is the possibility of recovering p from B with the help of the Minkowski functional, as stated in Theorem 2.

Definition 3. *A subset $B \subset \mathcal{X}$ of a topological vector space \mathcal{X} is called a disk if it is convex and center-symmetric. The Minkowski functional (or gauge) associated with such a disk B is*

$$\mu_B(x) = \inf\{\lambda \in \mathbb{R}_{>0} : x \in \lambda B\}, \quad (4)$$

with the convention that $\mu_B(x) = \infty$ when the infimum in (4) does not exist.

A set is said to be absorbing if, for any $x \in \mathcal{X}$, there exists some $r > 0$ such that $x \in \lambda B$ for all $|\lambda| > r$. In particular, if B is a disk, then it is absorbing if and only if it includes the origin as an interior point.

Theorem 2 ([41, p. 120-121,115-154]). *Let B be an absorbing disk in a topological vector space \mathcal{X} .*

1. *The functional μ_B specified by (4) is a seminorm on \mathcal{X} .*
2. *If $A = \{x \in \mathcal{X} : \mu_B(x) < 1\}$ and $C = \{x \in \mathcal{X} : \mu_B(x) \leq 1\}$, then $A \subseteq B \subseteq C$ and $\mu_A = \mu_B = \mu_C$. In particular, if B is open (in the topology of \mathcal{X}), then $A = B$. Likewise, if B is closed, then $B = C$.*
3. *The gauge μ_B is continuous on \mathcal{X} if and only if B is a neighborhood of 0 in \mathcal{X} .*
4. *The gauge μ_B is a norm on \mathcal{X} if and only if B does not contain any linear subspace of \mathcal{X} , except $\{0\}$.*

Conversely, let p be a (semi)norm on \mathcal{X} . Then, $B = \{x \in \mathcal{X} : p(x) \leq 1\}$ is convex, balanced, and absorbing with $p = \mu_B$.

The powerful aspect of this result is that the Banach disk B does not even need to be closed (see Item 2). We note that the fourth condition (induction of a norm) is automatically met if the set B in Theorem 2 is bounded. In such a scenario, B can be assimilated to the unit ball of the norm $\|\cdot\| = \mu_B(\cdot)$, while the determination of the norm for a particular

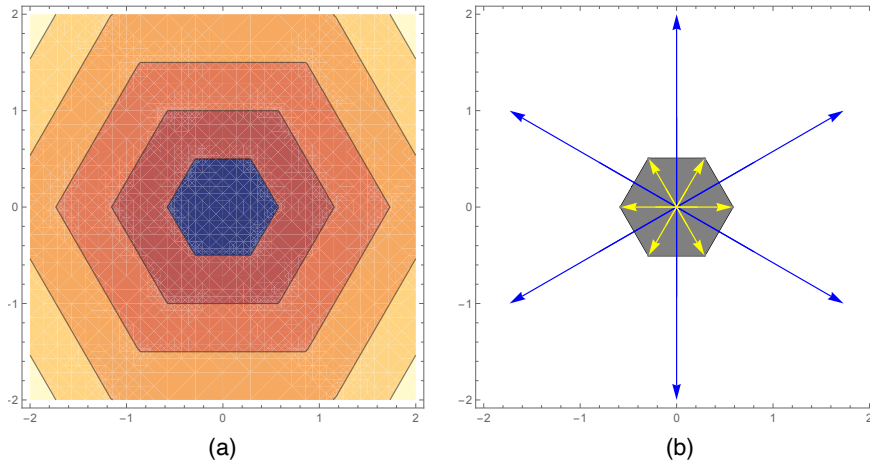


Figure 1: Unit ball of a polyhedral norm: (a) Contour plot of $\mathbf{x} \mapsto \|\mathbf{L}\mathbf{x}\|_{\ell_1}$ with the darker central region in the plane being the unit ball B_{p_1} . (b) Overlay of the vertex (yellow) and facet (blue) vectors, the latter being the normals of the supporting hyperplanes of B_{p_1} . XXX Adapt for B&W

point $x \in \mathcal{X}$ (see (4)) amounts to inflating B by λ (resp., deflating B if $\lambda < 1$) up to the limit point where x enters λB (resp, x leaves λB).

To illustrate the concept, we show the contour-plot of the sparsity-promoting regularizer $p_1(\mathbf{x}) = \|\mathbf{L}\mathbf{x}\|_{\ell_1}$ for $\mathbf{L} = \begin{pmatrix} 0 & 1 \\ -\frac{\sqrt{3}}{2} & -\frac{1}{2} \\ \frac{\sqrt{3}}{2} & -\frac{1}{2} \end{pmatrix} \in \mathbb{R}^{3 \times 2}$

in Figure 1. We observe that B_{p_1} is symmetric, convex and bounded, where the latter reflects the property that the underlying regularization operator is injective. These properties are characteristic of a norm, in conformity with Item 4 in Theorem 2. The unit ball of this particular norm has $N = 6$ extreme points/vertices $\mathbf{g}_1, \dots, \mathbf{g}_N$ (overlaid as light vectors), so that it can also be described as the *convex hull* of its vertices: $B_{p_1} = \text{Conv}\{\mathbf{g}_n\}_{n=1}^N$. We shall see that B_{p_1} also admits a dual representation as an intersection of half-spaces, whose normals (facet-vectors) are overlaid in blue.

3.2 Universal Parametric Polyhedral Regularizers

Theorem 1 implies that a convex equivariant regularization g on \mathbb{R}^d can be imposed via the minimization of a corresponding (semi)norm $p = p_{\theta}$. For mathematical convenience, we shall now restrict our attention to the Banach

setting where p is a norm that is characterized by its unit ball B_p . Since the latter is a convex, symmetric, and bounded subset of \mathbb{R}^d , it can itself be approximated arbitrarily closely by a convex symmetric polytope that has sufficiently many vertices. This process is supported by Theorem 2: to induce an equivalent (semi-)norm, it is sufficient to reproduce the unit ball of the regularizer. By searching among all convex symmetric polytopes, we are actually spanning the norms associated with the family of polyhedral Banach spaces (see Section 4.2). These spaces have some remarkable geometric properties, which are made explicit in Section 4 with the key results being summarized in Theorem 5.

We now present of variant of Theorem 5 that offers a practical answer to our design problem: a constructive parameterization of all polyhedral norms in terms of dictionaries or, alternatively, regularization operators.

Theorem 3 (Dual parameterization of all polyhedral norms). *Let us consider the two complementary functionals*

$$\mathbf{x} \mapsto \|\mathbf{x}\|_{\mathcal{S}, \mathbf{G}} = \min_{\mathbf{z} \in \mathbb{R}^{\tilde{N}}} \{\|\mathbf{z}\|_{\ell_1} : \mathbf{x} = \mathbf{G}\mathbf{z}\} \quad (5)$$

$$\mathbf{x} \mapsto \|\mathbf{x}\|_{\mathcal{A}, \mathbf{G}^\top} = \|\mathbf{G}^\top \mathbf{x}\|_{\ell_\infty} \quad (6)$$

parameterized by some rectangular matrix $\mathbf{G} = [\mathbf{g}_1 \ \dots \ \mathbf{g}_{\tilde{N}}] \in \mathbb{R}^{d \times \tilde{N}}$. These are norms on \mathbb{R}^d if and only if $\text{rank}(\mathbf{G}) = d$, in which case $\mathcal{X}_{\mathcal{S}} = (\mathbb{R}^d, \|\cdot\|_{\mathcal{S}, \mathbf{G}})$ and $\mathcal{X}_{\mathcal{A}} = (\mathbb{R}^d, \|\cdot\|_{\mathcal{A}, \mathbf{G}^\top})$ form a dual pair of polyhedral Banach spaces.

The two forms are universal: In either case, the matrix \mathbf{G} can be adjusted/trained to encode the norm of any polyhedral Banach space, with the complementary form yielding the dual norm. The underlying polyhedral geometry is determined solely by the “extreme points” of \mathbf{G} :

$$\{\mathbf{v}_1, \dots, \mathbf{v}_N\} = \text{Ext Conv}\{\pm \mathbf{g}_1, \dots, \pm \mathbf{g}_{\tilde{N}}\} = \text{Ext } \mathbf{G} \quad (7)$$

with $N \leq 2\tilde{N}$. These are the vertices of the unit ball of $\mathcal{X}_{\mathcal{S}}$ as well as the facet vectors of the unit ball of $\mathcal{X}_{\mathcal{A}}$, in conformity with the duality/polarity relations $\mathcal{X}_{\mathcal{A}} = \mathcal{X}'_{\mathcal{S}}$ and $B_{\mathcal{X}_{\mathcal{A}}} = B^\circ_{\mathcal{X}_{\mathcal{S}}}$ (see (44) in Appendix A).

Note that our definition of the extreme points of a dictionary in (7) includes some \pm signs. This is because the vertices necessarily appear in opposite pairs due to the symmetry of the underlying Banach disks. The process of the determination of the extreme points of a dictionary matrix \mathbf{G} is illustrated in Figure 2. The principle at work is that the induced unit regularization ball $B_{\mathcal{X}_{\mathcal{S}}}$ is the symmetric convex hull of the dictionary elements.

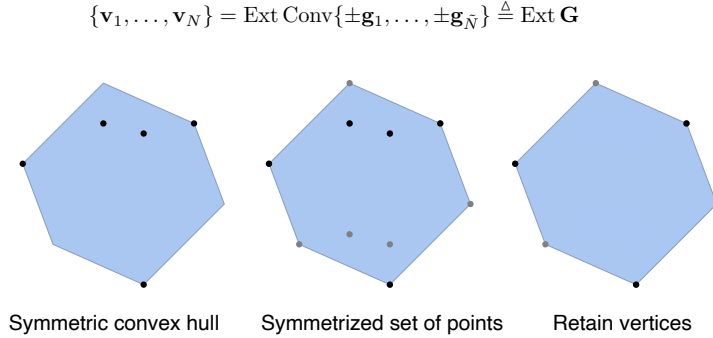


Figure 2: The extreme points of a matrix \mathbf{G} are given by the vertices of the symmetric convex hull of its column vectors represented as dark points on the left display.

Geometrically, the rank condition on \mathbf{G} in Theorem 3 translates into the unit ball $B_{\mathcal{X}_S}$ (or, equivalently, $B_{\mathcal{X}_A}$) being a bounded neighborhood of the origin, which is the necessary and sufficient condition to induce a norm (see Theorem 2, Item 4). This means that there is actually no restriction and that the scheme is capable of producing any desired vertical or facial configuration. Equation (7) also indicates that not all dictionary elements \mathbf{g}_n are active: the dictionary can be compressed by dropping elements that are not vertices or, otherwise, already represented by their signed counterpart. This reduction process ends when $N = 2\tilde{N}$, in which case the matrix \mathbf{G} in (7) is said to be *irreducible*.

By concentrating on the case of irreducible matrices and by invoking the property that any bounded set can be approximated to arbitrary precision by a polytope [42, 43], we are able to convert Theorem 3 into the universality result of Theorem 4.

Theorem 4 (Universality of polyhedral norm approximations). *Let $\|\cdot\|_{\mathcal{X}}$ be any norm on \mathbb{R}^d . Then, for any $\epsilon \in (0, 1)$, there exists some $\tilde{N} \geq d$ and an irreducible matrix $\mathbf{F} \in \mathbb{R}^{d \times \tilde{N}}$ such that*

$$\forall \mathbf{x} \in \mathbb{R}^d : \quad \frac{1}{1+\epsilon} \|\mathbf{x}\|_{\mathcal{X}} \leq \|\mathbf{F}^T \mathbf{x}\|_{\ell_\infty} \leq \frac{1}{1-\epsilon} \|\mathbf{x}\|_{\mathcal{X}}. \quad (8)$$

Likewise, there exists some $N \geq d$ and an irreducible matrix $\mathbf{V} \in \mathbb{R}^{d \times N}$ such that

$$\forall \mathbf{x} \in \mathbb{R}^d : \quad \frac{1}{1+\epsilon} \|\mathbf{x}\|_{\mathcal{X}} \leq \min_{\mathbf{z} \in \mathbb{R}^N} \{\|\mathbf{z}\|_{\ell_1} : \mathbf{x} = \mathbf{V}\mathbf{z}\} \leq \frac{1}{1-\epsilon} \|\mathbf{x}\|_{\mathcal{X}}. \quad (9)$$

Moreover, we have that $\epsilon = O\left(\frac{1}{n^{2/(d-1)}}\right)$, where $n = 2N$ is the number of extreme points of the underlying polyhedral unit ball $B = \text{Conv}(\mathbf{V})$ or $B = \{\mathbf{x} \in \mathbb{R}^d : \|\mathbf{F}^\top \mathbf{x}\|_{\ell_\infty} \leq 1\}$.

We note that the lower bounds in (8) and (9) imply that $\text{rank}(\mathbf{F}) = d$ and $\text{rank}(\mathbf{V}) = d$, respectively.

Proof. Let B be a convex, center-symmetric subset (i.e., a disk) of a Banach space \mathcal{X} that meets the inclusion conditions

$$B \subseteq C_0 B_{\mathcal{X}} = \{\mathbf{x} \in \mathbb{R}^d : \|\mathbf{x}\|_{\mathcal{X}} \leq C_0\} \quad \text{and} \quad B_{\mathcal{X}} \subseteq \frac{1}{c_0} B, \quad (10)$$

where $0 < c_0 \leq C_0$ are two constants. The right-hand side of (10) implies that B is absorbing, while the left-hand side tells us that B is bounded. This ensures that μ_B is a valid norm on \mathcal{X} (by Theorem 2). We then exploit the homogeneity of this norm to rewrite (10) as

$$\forall x \in \mathcal{X}, \quad c_0 \|x\|_{\mathcal{X}} \leq \mu_B(x) \leq C_0 \|x\|_{\mathcal{X}}, \quad (11)$$

which is the canonical way to indicate that the two norms are topologically equivalent.

In our case of interest, $\mathcal{X} = \mathbb{R}^d$ and B is the polyhedral unit ball induced by \mathbf{F} or \mathbf{V} , with \mathbf{V} having the capacity to encode all symmetric polytopes with $n = 2N$ vertices. Fixing n and viewing $B_{\mathcal{X}}$ as a bounded convex set, we can then invoke a classical result [44, 43] that states the existence of an approximating polytope B such that

$$d_H(B_{\mathcal{X}}, B) = \max \left\{ \sup_{\mathbf{x} \in B_{\mathcal{X}}} \inf_{\mathbf{y} \in B} \|\mathbf{x} - \mathbf{y}\|_2, \sup_{\mathbf{y} \in B} \inf_{\mathbf{x} \in B_{\mathcal{X}}} \|\mathbf{x} - \mathbf{y}\|_2 \right\} \leq \frac{C_{\mathcal{X}}}{n^{2/(d-1)}}, \quad (12)$$

where $d_H(B_{\mathcal{X}}, B)$ is the Hausdorff distance between $B_{\mathcal{X}}$ and B , and $C_{\mathcal{X}}$ is a constant that depends solely on $B_{\mathcal{X}}$. This means that one can make d_H arbitrarily small by selecting a dictionary that has sufficiently many extreme points or, equivalently, a regularization operator \mathbf{F}^\top that induces sufficiently many facets (see Theorem 5 for additional insights).

Since all finite-dimensional norms are equivalent, the estimate in (12) also holds if we substitute $\|\cdot\|_2$ by any other norm under some adaptation of the bounding constant $C_{\mathcal{X}}$. The form that is suitable for our purpose is

$$\begin{aligned} \tilde{d}_H(B_{\mathcal{X}}, B) &= \max \left\{ \sup_{\mathbf{x} \in B_{\mathcal{X}}} \inf_{\mathbf{y} \in B} \|\mathbf{x} - \mathbf{y}\|_{\mathcal{X}}, \sup_{\mathbf{y} \in B} \inf_{\mathbf{x} \in B_{\mathcal{X}}} \|\mathbf{x} - \mathbf{y}\|_{\mathcal{X}} \right\}, \\ &= \min\{\lambda \geq 0 : B_{\mathcal{X}} \subset B + \lambda B_{\mathcal{X}}, B \subset B_{\mathcal{X}} + \lambda B_{\mathcal{X}}\}. \end{aligned}$$

where the “+” symbol applied to sets denotes the Minkowski sum. The second form implies that $B \subset (1 + \tilde{d}_H)B_{\mathcal{X}}$ and $(1 - \tilde{d}_H)B_{\mathcal{X}} \subset B$ under the implicit assumption that $0 \leq \tilde{d}_H < 1$. We make the link with (10) by setting $c_0 = \frac{1}{1+\tilde{d}_H}$ and $C_0 = \frac{1}{1-\tilde{d}_H}$, with (11) then yielding the desired result. \square

4 Supporting Banach-Space Theory

4.1 Nomenclature and notation

We start by recalling a few geometric and topological concepts. Let $C \subset \mathbb{R}^d$ denote some proper subset of \mathbb{R}^d . Then, C said to be *convex* if and only if $\lambda \mathbf{x} + (1 - \lambda)\mathbf{y} \in C$ for all $\mathbf{x}, \mathbf{y} \in C$ and $\lambda \in [0, 1]$. Likewise, it is said to be *bounded* if there exists an Euclidean neighborhood $N(\mathbf{x}_0; R) = \{\mathbf{x} \in \mathbb{R}^d : \|\mathbf{x} - \mathbf{x}_0\|_2 \leq R\}$ of radius $R > 0$ and center \mathbf{x}_0 such that $C \subset N(\mathbf{x}_0; R)$. The set C is (topologically) *closed* if it contains all its boundary points or, equivalently, if its complement in \mathbb{R}^d is open. Since all finite-dimensional norms are equivalent, the closedness of C can be formalized as follows: for any $\mathbf{y} \notin C$, there exists some Euclidean neighborhood $N(\mathbf{y}, \epsilon)$ with $\epsilon > 0$ whose intersection with C is empty. In finite dimensions, there is also an equivalence between the mathematical notion of *compactness* and the property of being closed and bounded (Heine-Borel theorem).

A *disk* D is a convex, center-symmetric (or balanced) subset of \mathbb{R}^d . The prototypical example of a *compact disk* is the unit ball $B_{\mathcal{X}} = \{\mathbf{x} \in \mathbb{R}^d : \|\mathbf{x}\|_{\mathcal{X}} \leq 1\}$ associated with any admissible norm $\|\cdot\|_{\mathcal{X}}$ on \mathbb{R}^d .

A *polyhedron* $Q \subset \mathbb{R}^d$ is the intersection of a finite number (M) of half-spaces. Formally, $Q = \bigcap_{m=1}^M K(\mathbf{f}_m, \alpha_m)$, where

$$K(\mathbf{f}_m, \alpha_m) = \{\mathbf{x} \in \mathbb{R}^d : \langle \mathbf{f}_m, \mathbf{x} \rangle \leq \alpha_m\} \quad (13)$$

is a half-space characterized by its outward normal vector $\mathbf{f}_m \in \mathbb{R}^d$ (which may or may not be normalized) and an offset $\alpha_m \in \mathbb{R}$. The representation is called *irreducible* when the number of half-spaces M is minimal. In such a scenario, the corresponding hyperplanes

$$H(\mathbf{f}_m, \alpha_m) = \{\mathbf{x} \in \mathbb{R}^d : \langle \mathbf{f}_m, \mathbf{x} \rangle = \alpha_m\} \quad (14)$$

outline the boundary of Q and are called the *supporting hyperplanes* of the polyhedron. The boundary of the polyhedron can then be subdivided into M facets $F_m = Q \cap H(\mathbf{f}_m, \alpha_m)$, each of which is the intersection of the body and its corresponding supporting hyperplane.

A *convex polytope* P is the *convex hull* of a finite number (K) of points, which is written as $P = \text{Conv}\{\mathbf{p}_1, \dots, \mathbf{p}_K\}$ with $\mathbf{p}_k \in \mathbb{R}^d$. Alternatively, P can be described as a convex compact subset of \mathbb{R}^d that has a finite number of *extreme points*. These extreme points are $\text{Ext}P = \{\mathbf{v}_1, \dots, \mathbf{v}_N\}$ with $N \leq K$; they are the *vertices* of the polytope. They necessarily form a subset of the \mathbf{p}_k 's in the first definition and yield the most concise (irreducible) representation of the polytope as $P = \text{Conv}\{\mathbf{v}_n\}_{n=1}^N$.

The fundamental theorem for polytopes states that every bounded polyhedron is a convex polytope and vice versa [45]. In fact, as we shall see, the two representations are related by duality, which also means that it is always possible to switch from one to the other and to use the one that is the most appropriate for a given task or mathematical derivation.

4.2 Polyhedral Banach Spaces

We now present the theoretical framework that supports the derivation of Theorem 3 through the characterization of all Banach spaces whose unit balls have a finite number of extreme points¹. Klee calls a Banach space \mathcal{X} polyhedral if the unit ball of every finite-dimensional subspace of \mathcal{X} is a polyhedron [46]. After having identified $c_0(\mathbb{N})$ as the (infinite-dimensional) prototype of such spaces, he asked whether there also exist some infinite-dimensional polyhedral spaces that are reflexive. Lindenstrauss then showed the impossibility of such a construction by proving that there is no infinite-dimensional conjugate space \mathcal{X}' that is polyhedral [47]. In particular, this implies that $\ell_1(\mathbb{N}) = (c_0(\mathbb{N}))'$ is not polyhedral in the strict sense of the term.

Fortunately for us, the situation is much more favorable in finite dimensions where all Banach spaces are reflexive and where the duals of polyhedral spaces are polyhedral as well.

Definition 4. *A finite-dimensional Banach space \mathcal{X} is said to be polyhedral if its unit ball $B_{\mathcal{X}}$ has a finite number of extreme points.*

Since $B_{\mathcal{X}}$ is compact by construction, it is the convex hull of its extreme points and, hence, a polyhedron (or polytope), which justifies the nomenclature. In the geometric context of polytopes, these extreme points are called vertices, and one can then take advantage of all the mathematical tools available in this area.

¹Geometrically, this is equivalent to $B_{\mathcal{X}}$ being a convex, symmetric polytope (see Appendix A).

The next theorem expresses the remarkable consequences of the association between the vertices (resp., the facets) of $B_{\mathcal{X}}$ and the facets (resp., vertices) of the unit ball of its topological dual. Most of the results in Theorem 5 are standard in the theory of convex polytopes [45, 48, 49], even though they are rarely stated in the present format (Banach setting). That said, we are unaware of a published mention of the S-form of the norm (Item 4, see our proof below). This S-form is crucial to our formulation.

Definition 5. A collection $\{\mathbf{v}_1, \dots, \mathbf{v}_N\}$ of vectors (vertices or facet-normals) is said to be irreducible if $\text{Ext Conv}\{\mathbf{v}_1, \dots, \mathbf{v}_N\} = \{\mathbf{v}_1, \dots, \mathbf{v}_N\}$.

If a given collection of vectors (or dictionary elements) does not meet the above condition, then one can apply a standard procedure to reduce it to a (unique) minimal set, which is formed by the vertices of its convex hull.

Theorem 5 (Geometry of polyhedral Banach spaces). *Let $\mathcal{X} = (\mathbb{R}^d, \|\cdot\|_{\mathcal{X}})$ and $\mathcal{X}' = (\mathbb{R}^d, \|\cdot\|_{\mathcal{X}'})$ be a dual pair of polyhedral Banach spaces. Then, the Banach topology of \mathcal{X} has the following equivalent geometric descriptions in terms of (irreducible) vertices or facet-vectors.*

1. $\|\cdot\|_{\mathcal{X}} = \mu_{B_{\mathcal{X}}}(\cdot)$ where the polyhedral unit ball $B_{\mathcal{X}}$ is the convex hull of its vertices $\{\mathbf{v}_1, \dots, \mathbf{v}_N\} = \text{Ext}B_{\mathcal{X}}$ with $N > d$, which leads to

$$\begin{aligned} B_{\mathcal{X}} &= \text{Conv}\{\mathbf{v}_1, \dots, \mathbf{v}_N\} \\ &= \left\{ \mathbf{x} = \sum_{n=1}^N \lambda_n \mathbf{v}_n : \lambda_n \geq 0 \text{ for all } n \text{ and } \sum_{n=1}^N \lambda_n = 1 \right\}. \end{aligned} \quad (15)$$

2. $\|\cdot\|_{\mathcal{X}} = \mu_{B_{\mathcal{X}}}(\cdot)$ where $B_{\mathcal{X}}$ is an intersection of M half-spaces given by

$$B_{\mathcal{X}} = \bigcap_{m=1}^M K(\mathbf{f}_m, 1) = \{ \mathbf{x} \in \mathbb{R}^d : \langle \mathbf{f}_m, \mathbf{x} \rangle \leq 1 \text{ for all } m \}, \quad (16)$$

with the \mathbf{f}_m (facet-vectors) being the directed normals of the facets $F(\mathbf{f}_m) = H(\mathbf{f}_m, 1) \cap B_{\mathcal{X}}$ of $B_{\mathcal{X}}$.

3. Analysis form of the norm with $\mathbf{F} = [\mathbf{f}_1 \cdots \mathbf{f}_M] \in \mathbb{R}^{d \times M}$:

$$\|\mathbf{x}\|_{\mathcal{X}} = \max\{|\langle \mathbf{f}_m, \mathbf{x} \rangle|\}_{m=1}^M = \|\mathbf{F}^T \mathbf{x}\|_{\ell_{\infty}}. \quad (17)$$

4. Synthesis form of the norm with $\mathbf{V} = [\mathbf{v}_1 \cdots \mathbf{v}_N] \in \mathbb{R}^{d \times N}$:

$$\|\mathbf{x}\|_{\mathcal{X}} = \min_{\mathbf{z} \in \mathbb{R}^M} \{ \|\mathbf{z}\|_{\ell_1} : \mathbf{x} = \mathbf{V}\mathbf{z} \}. \quad (18)$$

The same relations hold for the dual norm with the role of the vertices and facets being interchanged. For instance, we have that

$$\begin{aligned} B_{\mathcal{X}'} &= \text{Conv}\{\mathbf{f}_1, \dots, \mathbf{f}_M\} \\ &= \bigcap_{n=1}^N K(\mathbf{v}_n, 1) = \{\mathbf{y} \in \mathbb{R}^d : \|\mathbf{y}\|_{\mathcal{X}'} = \|\mathbf{V}^\top \mathbf{y}\|_{\ell_\infty} \leq 1\}. \end{aligned} \quad (19)$$

This duality is exemplified by the relation

$$\forall(\mathbf{x}, \mathbf{f}_m) \in B_{\mathcal{X}} \times \text{Ext}B_{\mathcal{X}'}, \quad -1 \leq \langle \mathbf{f}_m, \mathbf{x} \rangle \leq 1 \quad (20)$$

with the upper/lower bound being achieved if and only if $\mathbf{x} \in F(\pm \mathbf{f}_n)$ with $F(\mathbf{f}_n) = B_{\mathcal{X}} \cap H(\mathbf{f}_n, 1)$ being the facet with normal vector \mathbf{f}_m .

Proof.

Item 1. We can either view (15) as the definition of a convex polygon or as a consequence of the Krein-Milman theorem which states that any compact convex set is the convex hull of its extreme points, with the latter being the vertices of $B_{\mathcal{X}}$. One then recovers the norm by taking the Minkowski functional of $B_{\mathcal{X}}$ (see Theorem 2).

Item 2. Here, we invoke the fundamental theorem for polytopes [45, Theorem 1.1, p. 29] which states the equivalence between the vertex-based and facial representations of a polytope.

Item 3. The symmetry of the $B_{\mathcal{X}}$ (Banach disk) implies that its facet-vectors necessarily come in (signed) pairs $\pm \mathbf{f}_n$. We then identify the unit ball $\{\mathbf{x} \in \mathbb{R}^d : \|\mathbf{F}^\top \mathbf{x}\|_{\ell_\infty} \leq 1\}$ as the convex set specified by (16) by observing that $K(\mathbf{f}_m, 1) \cap K(-\mathbf{f}_m, 1) = \{\mathbf{x} \in \mathbb{R}^d : |\langle \mathbf{f}_m, \mathbf{x} \rangle| \leq 1\}$. Since the unit balls are the same, the induced norms are identical, as direct consequence of Theorem 2.

Item 4. For any $\mathbf{x} \in \mathbb{R}^d \setminus \{\mathbf{0}\}$, we have that $\frac{\mathbf{x}}{\|\mathbf{x}\|_{\mathcal{X}}} \in B_{\mathcal{X}}$ which, in view of (15), implies the existence of some $\mathbf{z} = \|\mathbf{x}\|_{\mathcal{X}}(\lambda_1, \dots, \lambda_N) \in \mathbb{R}^N$ such that $\mathbf{x} = \mathbf{V}\mathbf{z}$ with $\|\mathbf{z}\|_{\ell_1} = \|\mathbf{x}\|_{\mathcal{X}} \sum_{n=1}^N |\lambda_n| = \|\mathbf{x}\|_{\mathcal{X}}$. This proves that the functional $p(\mathbf{x}) = \min\{\|\mathbf{z}\|_{\ell_1} : \mathbf{x} = \mathbf{V}\mathbf{z}\}$ is well-defined with $p(\mathbf{x}) \leq \|\mathbf{x}\|_{\mathcal{X}}$.

As next step, we show that p specifies a norm on \mathbb{R}^d . Let $\mathbf{x}^* \in \mathbb{R}^N$ be an optimal code for $\mathbf{x} \in \mathbb{R}^d$ (not necessarily unique) such that $\mathbf{x} = \mathbf{V}\mathbf{x}^*$ and $p(\mathbf{x}) = \|\mathbf{x}^*\|_{\ell_1}$. Since the ℓ_1 -norm and the linear constraint are both renormalizable, we readily deduce that $\alpha \mathbf{x}^*$ is an optimal code for $\alpha \mathbf{x}$ for any $\alpha \in \mathbb{R}$, which yields $p(\alpha \mathbf{x}) = \|\alpha \mathbf{x}^*\|_{\ell_1} = |\alpha| \|\mathbf{x}^*\|_{\ell_1} = |\alpha| p(\mathbf{x})$ (homogeneity). Likewise, since the determination of p involves an minimum

over all possible generative scenarios, we have that $\mathbf{x} = \mathbf{0} \Leftrightarrow p(\mathbf{x}) = \|\mathbf{0}\|_{\ell_1}$ (positive definiteness). Finally, let \mathbf{x}_1^* and \mathbf{x}_2^* be optimal codes for \mathbf{x}_1 and \mathbf{x}_2 , respectively. Then, by linearity, we have that $\mathbf{x}_1 + \mathbf{x}_2 = \mathbf{V}(\mathbf{x}_1^* + \mathbf{x}_2^*)$, so that

$$p(\mathbf{x}_1 + \mathbf{x}_2) \leq \|\mathbf{x}_1^* + \mathbf{x}_2^*\|_{\ell_1} \leq \|\mathbf{x}_1^*\|_{\ell_1} + \|\mathbf{x}_2^*\|_{\ell_1} = p(\mathbf{x}_1) + p(\mathbf{x}_2) \quad (21)$$

is the desired triangle inequality. Hence, $\mathcal{X}_p = (\mathbb{R}^d, p(\cdot))$ is a Banach space. This allows us to interpret the linear map $\mathbf{z} \mapsto \mathbf{V}\{\mathbf{z}\} = \mathbf{V}\mathbf{z}$ as a continuous surjection $\mathbf{V} : \ell_1(\mathbb{I}) \rightarrow \mathcal{X}_p$ with $\|\mathbf{V}\| = 1$ (by construction). This tells us that the operator \mathbf{V} is a projective isometry that maps the unit ball of $\ell_1(\mathbb{I})$ onto the unit ball of \mathcal{X}_p . Accordingly, we have that $B_{\mathcal{X}_p} = \mathbf{V}(B_{\ell_1(\mathbb{I})}) = \mathbf{V}\left(\text{Conv}\{\pm \mathbf{e}_n\}_{n=1}^N\right) = \text{Conv}\{\pm \mathbf{V}\mathbf{e}_n\}_{n=1}^N = \text{Conv}\{\pm \mathbf{v}_n\}_{n=1}^N$. Since the vertices \mathbf{v}_n come in pairs (due to the symmetry of $B_{\mathcal{X}}$), we have that

$$\text{Ext}B_{\mathcal{X}_p} = \text{Ext} \text{Conv}\{\pm \mathbf{v}_n\}_{n=1}^N = \{\mathbf{v}_n\}_{n=1}^N. \quad (22)$$

This proves that the unit balls of \mathcal{X}_p and \mathcal{X} (and, hence, the induced norms) are identical.

Duality between vertices and facets: This is a central theme in the theory of polytope that goes under the name of polarity [49, Theorem 9.1, p. 57]. When applied to the present setting, the polarity theorem for polytopes implies that $B_{\mathcal{X}'} = B_{\mathcal{X}}^\circ = \bigcap_{n=1}^N K(\mathbf{v}_n, 1)$ is the polar of $B_{\mathcal{X}} = \text{Conv}\{\mathbf{v}_1, \dots, \mathbf{v}_N\}$, while $B_{\mathcal{X}} = B_{\mathcal{X}'}^{\circ\circ} = B_{\mathcal{X}'}^\circ = \bigcap_{n=1}^N K(\mathbf{f}_n, 1)$ is the polar of $B_{\mathcal{X}} = \text{Conv}\{\mathbf{v}_1, \dots, \mathbf{v}_N\}$. (In the finite-dimensional setting, all Banach spaces are reflexive with $B_{\mathcal{X}} = B_{\mathcal{X}''}$, which makes the definition of polarity—see (44) in the appendix—compatible with that of Banach duality.) In view of the argumentation in Item 3, the polyhedral representation of $B_{\mathcal{X}}$ is equivalent to $B_{\mathcal{X}} = \{\mathbf{x} \in \mathbb{R}^d : \max\{|\langle \mathbf{f}_m, \mathbf{x} \rangle| \leq 1\}_{m=1}^M\}$, which implies (20). The equality holds for $\langle \mathbf{f}_m, \mathbf{x} \rangle = \pm 1$, which happens if and only if $\mathbf{x} \in B_{\mathcal{X}} \cap H(\mathbf{f}_m, 1)$ or $\mathbf{x} \in B_{\mathcal{X}} \cap H(-\mathbf{f}_m, 1) = F(-\mathbf{f}_m)$, where $H(\mathbf{f}_m, 1)$ is the supporting hyperplane with outward normal vector \mathbf{f}_m . □

The geometric interpretation of (20) is that \mathbf{f}_m , which is now identified as a vertex of $B_{\mathcal{X}'}$, is the common Banach conjugate² of all boundary points lying on the corresponding facet of $B_{\mathcal{X}}$.

²The general duality inequality for Banach spaces is $|\langle x, y \rangle| \leq \|x\|_{\mathcal{X}} \|y\|_{\mathcal{X}'}$ for all $(x, y) \in \mathcal{X} \times \mathcal{X}'$. Two such elements are said to be Banach conjugates if they saturate the inequality with $\langle x, y \rangle = \|x\|_{\mathcal{X}} \|y\|_{\mathcal{X}'}$.

An important observation is that (17) and (18) also hold for “non-minimal” sets of vertices/facets. Indeed, the enabling property that yields the equivalence of norms in the proof of Theorem 5 is the preservation of the underlying convex hull(s). This naturally leads to the statement of the more practical variant of the characterization in Theorem 3. Likewise, because of the presence of the absolute value in the underlying norms, it is possible to reduce the width of the matrices \mathbf{V} and \mathbf{F} in (17) and (18) by two, so that

$$\begin{aligned}\|\mathbf{x}\|_{\mathcal{X}} &= \min_{\mathbf{z} \in \mathbb{R}^M} \{\|\mathbf{z}\|_{\ell_1} : \mathbf{x} = \mathbf{V}_+ \mathbf{z}\} \\ &= \|\mathbf{F}_+^T \mathbf{x}\|_{\ell_\infty}\end{aligned}\tag{23}$$

with $\mathbf{V}_+ \in \mathbb{R}^{d \times N/2}$ and $\mathbf{F}_+ \in \mathbb{R}^{d \times M/2}$, which are the two concrete forms that will be referred to as “irreducible.”

It is instructive to apply Theorem 5 to $\mathcal{X} = \ell_1(\mathbb{I}) = (\mathbb{R}^N, \|\cdot\|_{\ell_1})$. The corresponding unit ball is the famous cross-polytope, which has the following two equivalent representations:

$$B_{\ell_1} = \text{Conv}\{\pm \mathbf{e}_1, \dots, \pm \mathbf{e}_N\}\tag{24}$$

$$= \left\{ \mathbf{x} \in \mathbb{R}^N : \sum_{n=1}^N b_n x_n \leq 1 \text{ for all } b_1, \dots, b_N \in \{-1, +1\} \right\},\tag{25}$$

where \mathbf{e}_n denotes the n th element of the canonical basis. Equation (24) explicitly lists its $2N$ vertices (extreme points), while (25) shows the $M = 2^N$ supporting planes that specify its facets. In this basic scenario, the S-form of the norm is simply $\|\mathbf{x}\|_{\mathcal{X}} = \|\mathbf{x}\|_{\ell_1}$, while its A-form is

$$\|\mathbf{x}\|_{\ell_1} = \|\mathbf{B}_N^T \mathbf{x}\|_{\ell_\infty},\tag{26}$$

where $\mathbf{B}_N = [\mathbf{b}_1 \ \dots \ \mathbf{b}_{2^N}] \in \mathbb{R}^{N \times 2^N}$ is the matrix representation of all “binary” vectors \mathbf{b}_m in (25) with components in $\{-1, 1\}$. The theoretical relevance of (26) is the possibility of the representation an ℓ_1 -norm by an ℓ_∞ -norm, while the reverse generally does not hold for $N > 2$.

The dual of $\ell_1(\mathbb{I})$ is $\mathcal{X}' = \ell_\infty(\mathbb{I}) = (\mathbb{R}^N, \|\cdot\|_{\ell_\infty})$ whose unit ball is the N -dimensional hypercubic B_{ℓ_∞} , which has 2^N binary vertices \mathbf{b}_m and $2N$ facets with normal vectors $\pm \mathbf{e}_n$. In this scenario, it is the S-form

$$\|\mathbf{x}\|_{\ell_\infty} = \min_{\mathbf{z} \in \mathbb{R}^{2^N}} \{\|\mathbf{z}\|_{\ell_1} : \mathbf{x} = \mathbf{B}_N \mathbf{z}\},\tag{27}$$

that is non-standard, while the A-form reverts to the classical formula.

5 Parametric Reconstruction Pipelines

Given the constraint of an equivariant regularizer g , we now use Theorems 3 and 4 to specify some polyhedral approximation(s) of the generic variational signal-reconstruction problem (1). We shall consider three architectures, with the third being the one that presently lends itself the best to training.

5.1 Sparse Encoding in a Frame/Dictionary

The first form in Theorem 3, together with the universality result (9), suggests the reformulation of our problem as

$$S_I = \{\tilde{\mathbf{s}} \in \arg \min_{\mathbf{s} \in \mathbb{R}^d} (\frac{1}{2} \|\mathbf{y} - \mathbf{H}\mathbf{s}\|_2^2 + \lambda \|\mathbf{s}\|_{\mathbf{S}, \mathbf{G}})\}, \quad (28)$$

where the underlying regularizer—the synthesis norm defined by (5)—is parameterized by the matrix $\mathbf{G} \in \mathbb{R}^{d \times N}$. The literal form (28) involves two nested optimizations: an outer one to minimize the overall cost, and an inner one to evaluate $\|\mathbf{s}\|_{\mathbf{S}, \mathbf{G}}$ for every candidate \mathbf{s} , which, according to the definition, requires the determination of an optimal codeword in the dictionary \mathbf{G} . Fortunately, we can simplify the task by setting $\mathbf{s} = \mathbf{G}\mathbf{z}$ and recasting (28) in terms of the auxiliary codeword variable $\mathbf{z} \in \mathbb{R}^N$. After substitution and mutualization of the minimization, this results in

$$S_I = \{\tilde{\mathbf{s}} = \mathbf{G}\tilde{\mathbf{z}} : \tilde{\mathbf{z}} \in \arg \min_{\mathbf{z} \in \mathbb{R}^N} \frac{1}{2} \|\mathbf{y} - \mathbf{H}\mathbf{G}\mathbf{z}\|_2^2 + \lambda \|\mathbf{z}\|_{\ell_1}\}, \quad (29)$$

which has a strong feel of “déjà vu.” Indeed, (29) is the standard “synthesis form” (a.k.a. sparse encoding) used in compressed sensing [39], for which a multitude of efficient iterative solvers have been developed. The present contribution is the proof that (29) with a learnable dictionary \mathbf{G} , as advocated in [38], is universal for the class of equivariant convex regularizers.

We have already hinted to the property that the matrix $\mathbf{G} = [\mathbf{g}_1 \cdots \mathbf{g}_N]$ defines a dictionary with atoms $\mathbf{g}_n \in \mathbb{R}^d$. The admissibility condition $\text{rank}(\mathbf{G}) = d$ in Theorem 3 implies that the \mathbf{g}_n form a frame of \mathbb{R}^d [50]. This means that there exist two constants A and B such that

$$\mathbf{s} \in \mathbb{R}^d : \quad A \|\mathbf{s}\|_2^2 \leq \sum_{n=1}^N |\langle \mathbf{s}, \mathbf{g}_n \rangle|^2 \leq B \|\mathbf{s}\|_2^2. \quad (30)$$

The optimal frame bounds A and B are the minimum and maximum eigenvalues of the frame operator $\mathbf{s} \mapsto \sum_{n=1}^N \mathbf{g}_n \langle \mathbf{s}, \mathbf{g}_n \rangle = \mathbf{A}\mathbf{s}$, with $\mathbf{A} = \mathbf{G}\mathbf{G}^T \in \mathbb{R}^{d \times d}$ [50].

To ensure that all the elements of the dictionary are extreme points (irreducible scenario), we propose to impose the normalization constraint $\|\mathbf{g}_n\|_2 = 1$. Indeed, the strong convexity of $\mathbf{z} \mapsto \|\mathbf{z}\|_2^2$ implies that $\|\lambda\mathbf{g}_n + (1 - \lambda)\mathbf{g}_{n'}\|_2^2 < \lambda\|\mathbf{g}_n\|_2^2 + (1 - \lambda)\|\mathbf{g}_{n'}\|_2^2 = 1$, for any $\lambda \in]0, 1[$ and $\mathbf{g}_n \neq \mathbf{g}_{n'}$. This means that all non-extreme points $\mathbf{g} \in \text{conv}\{\pm\mathbf{g}_1, \dots, \pm\mathbf{g}_N\}$ that are in the symmetric convex hull of the \mathbf{g}_n have an ℓ_2 -norm that is smaller than 1. We can then insert a new element \mathbf{g}_{N+1} with $\|\mathbf{g}_{N+1}\|_2 = 1$ without spoiling the extreme-point properties of the others.

While (29) is very attractive for inference because of the availability of efficient resolution methods when the dictionary is known, it is much harder to optimize over \mathbf{G} in order to learn the “optimal” dictionary for a given class of signals, also in the simpler denoising scenario ($\mathbf{H} = \mathbf{I}_d$) commonly used for training. We attribute this state of affairs, which is well documented in the literature [51, 52, 53], to the fact that \mathbf{G} has a huge null space (of dimension $N - d$), which makes the optimization difficult and costly. There is also the necessity to maintain the condition $\text{rank}(\mathbf{G}) = d$ to ensure that (29) with \mathbf{G} fixed is well-posed.

5.2 Universal Weighted ℓ_∞ -Regularization

The optimization problem associated with the second form in Theorem 3 is

$$S_{\text{II}} = \{\tilde{\mathbf{s}} \in \arg \min_{\mathbf{s} \in \mathbb{R}^d} \frac{1}{2} \|\mathbf{y} - \mathbf{H}\mathbf{s}\|_2^2 + \lambda \|\mathbf{F}^T \mathbf{s}\|_{\ell_\infty}\} \quad (31)$$

where we are now using a distinct symbol for the regularization matrix $\mathbf{F} = [\mathbf{f}_1 \cdots \mathbf{f}_{\tilde{N}}] \in \mathbb{R}^{d \times \tilde{N}}$ formed from the facet vectors \mathbf{f}_n of the unit ball $B_{\mathcal{X}_S}$. Here too, (31) is reminiscent of the regularization methods used in compressed sensing, with the important difference that the regularizer now involves an ℓ_∞ -norm. Since the proximity operator $\|\cdot\|_{\ell_\infty}$ (adaptive soft-clip) is (almost) as convenient as that of $\|\cdot\|_{\ell_1}$ (soft-threshold), it is possible to adapt all the traditional algorithms (e.g., FISTA or ADMM) for the resolution of (31) with \mathbf{F}^T fixed.

Observe that (31) is conceptually simpler and less constraining than (29) because there is no (higher-dimensional) auxiliary variable \mathbf{z} nor any issue with some hidden null space. In fact, the scheme has the capacity to encode all seminorms if one drops the rank constraint on \mathbf{F} .

As for training, it can in principle be achieved based on a classic regression task where \mathbf{F}^T is optimized for the minimum mean-square error denoising ($\mathbf{H} = \mathbf{I}_d$) of a representative set of images. The caveat is that the back-propagation of the gradient (training error) to the regularization

weights will be very slow because of the underlying ℓ_∞ -norm acting as a binary switch. Finding a way around this limitation is a topic that deserves further investigation because (31) is our most expressive convex architecture.

5.3 Weighted ℓ_1 -Regularization Revisited

Due to the difficulties encountered with the training of the two aforementioned architectures, we decided to revisit the regularization setup more typical of compressed sensing; namely,

$$\tilde{S}_1 = \arg \min_{\mathbf{s} \in \mathbb{R}^d} \frac{1}{2} \|\mathbf{y} - \mathbf{H}\mathbf{s}\|_2^2 + \lambda \|\mathbf{L}\mathbf{s}\|_{\ell_1} \quad (32)$$

which involves an operator $\mathbf{L} \in \mathbb{R}^{N \times d}$ with $N \geq d$ and a ℓ_1 -penalty instead of the less standard ℓ_∞ -norm in (31). We now show that (32) with trainable \mathbf{L} constitutes a valid alternative to (28) or (31) in the sense that it also induces a polyhedral regularization.

Proposition 1. *The functional $p(\mathbf{s}) = \|\mathbf{L}\mathbf{s}\|_{\ell_1}$ with $\mathbf{L} \in \mathbb{R}^{N \times d}$ is a polyhedral norm if and only if $\text{rank}(\mathbf{L}) = d$.*

Proof. The key here is to use (26) to express the functional as $p(\mathbf{s}) = \|\mathbf{B}_N^\top \mathbf{L}\mathbf{s}\|_{\ell_\infty} = \|\mathbf{G}^\top \mathbf{s}\|_{\ell_\infty}$ with $\mathbf{G}^\top = \mathbf{B}_N^\top \mathbf{L} \in \mathbb{R}^{M \times N}$, where $\mathbf{B}_N \in \mathbb{R}^{N \times M}$ is the binary matrix whose column vectors are the $M = 2^N$ vertices of the ℓ_∞ unit ball (hypercube) in N dimensions. The validity of (26) for all $\mathbf{x} \in \mathbb{R}^N$ also implies that \mathbf{B}_N^\top has full row rank (i.e., $\text{rank}(\mathbf{B}_N^\top) = N$), as it would not yield a norm otherwise. Since the left multiplication with such a matrix is rank-preserving [54, p. 96], one has that $\text{rank}(\mathbf{B}_N^\top \mathbf{L}) = \text{rank}(\mathbf{L}) \leq d$. We know from Theorem 3 that $p(\mathbf{s}) = \|\mathbf{G}^\top \mathbf{s}\|_{\ell_\infty}$ induces a polyhedral norm if and only if $\text{rank}(\mathbf{G}) = d$. Since $\text{rank}(\mathbf{G}^\top) = \text{rank}(\mathbf{G})$ is equal to $\text{rank}(\mathbf{L})$ in the present setting, this is the desired result. \square

Note that the matrix \mathbf{G} identified in the proof of Proposition 1 yields the explicit description of the underlying unit ball, as formulated in the final part of Theorem 3; that is, the canonical polyhedral form (16) with $\mathbf{F} = \text{Ext}(\mathbf{G}) = [\mathbf{f}_1 \cdots \mathbf{f}_M]$. This is illustrated in Figure 1b with the facet vectors \mathbf{f}_m being overlaid.

The only limitation of the parameterization suggested by Proposition 1 with trainable \mathbf{L} is that it is probably not universal. Yet, we can make an interesting connection with the synthesis formulation in (29): The rank condition in Proposition 1 guarantees the existence of a generalized inverse matrix $\tilde{\mathbf{G}} = [\tilde{\mathbf{g}}_1 \cdots \tilde{\mathbf{g}}_N] \in \mathbb{R}^{d \times N}$ (not necessarily unique) such that

$$\tilde{\mathbf{G}}\mathbf{L} = \mathbf{I}_d, \quad (33)$$

with the canonical solution being the pseudo-inverse $\tilde{\mathbf{G}} = \mathbf{L}^\dagger = (\mathbf{L}^\top \mathbf{L})^{-1} \mathbf{L}^\top$. By making the change of variable $\mathbf{z} = \mathbf{L}\mathbf{s}$ in (32) and by observing that $\tilde{\mathbf{G}}$ is a valid (bilateral) inverse of \mathbf{L} as long as its domain is restricted to $\text{Ran}(\mathbf{L}) = \{\mathbf{z} = \mathbf{L}\mathbf{s} : \mathbf{s} \in \mathbb{R}^d\}$, we get

$$\tilde{S}_I = \{\tilde{\mathbf{s}} = \tilde{\mathbf{G}}\tilde{\mathbf{z}} : \tilde{\mathbf{z}} \in \arg \min_{\mathbf{z} \in \text{Ran}(\mathbf{L})} \frac{1}{2} \|\mathbf{y} - \mathbf{H}\tilde{\mathbf{G}}\mathbf{z}\|_2^2 + \lambda \|\mathbf{z}\|_{\ell_1}\}, \quad (34)$$

which is almost the same as (28), except for the restriction on the search space for \mathbf{z} . While the latter results in some loss of expressivity, it has the advantage of making the training of $\tilde{\mathbf{G}}$ much better posed by getting rid of the aforementioned “nontrivial null space” problem.

To demonstrate our point, we now concentrate on the scenario where the regularization operator can be factorized as $\mathbf{L} = \mathbf{\Lambda} \mathbf{T}_\theta^\top$, where $\mathbf{\Lambda} = \text{diag}(\lambda_1, \dots, \lambda_N)$ is a diagonal matrix of adjustable weights with $\lambda_n > 0$ and $\mathbf{T}_\theta \in \mathbb{R}^{d \times N}$ is a tight frame parameterized by θ . The defining property here is $\mathbf{T}_\theta \mathbf{T}_\theta^\top = \mathbf{I}_d$, which makes the inversion process straightforward. By using the same technique as in the derivation of (34), we reformulate (32) as

$$S_{\text{III}} = \{\tilde{\mathbf{s}} = \mathbf{T}_\theta \tilde{\mathbf{z}} : \tilde{\mathbf{z}} \in \arg \min_{\mathbf{z} \in \text{Ran}(\mathbf{T}_\theta^\top)} \frac{1}{2} \|\mathbf{y} - \mathbf{H}\mathbf{T}_\theta \mathbf{z}\|_2^2 + \|\mathbf{\Lambda} \mathbf{z}\|_{\ell_1}\}. \quad (35)$$

Next, we define the barrier functional

$$i_{\mathbf{T}_\theta^\top}(\mathbf{z}) = \begin{cases} 0, & \text{if } \mathbf{z} \in \text{Ran}(\mathbf{T}_\theta^\top) = \{\mathbf{z} \in \mathbb{R}^N : \mathbf{T}_\theta^\top \mathbf{T}_\theta \mathbf{z} = \mathbf{z}\} \\ +\infty, & \text{otherwise} \end{cases} \quad (36)$$

which is lower semicontinuous and convex. With the help of the latter, we recast (35) as

$$S_{\text{III}} = \{\tilde{\mathbf{s}} = \mathbf{T}_\theta \tilde{\mathbf{z}} : \tilde{\mathbf{z}} \in \arg \min_{\mathbf{z} \in \mathbb{R}^N} \frac{1}{2} \|\mathbf{y} - \mathbf{H}\mathbf{T}_\theta \mathbf{z}\|_2^2 + i_{\mathbf{T}_\theta^\top}(\mathbf{z}) + \|\mathbf{\Lambda} \mathbf{z}\|_{\ell_1}\} \quad (37)$$

which is easier to minimize because the constraint on the search space has been removed.

5.4 Implementation of a Trainable Convex Regularizer

A standard requirement in computational imaging is that the regularizer be shift-invariant. In the context of (32), this is achieved by employing an N_{chan} -channel filterbank as the operator \mathbf{L} . This takes $\mathbf{s} \in \mathbb{R}^d$ as input and produces N_{chan} output channels, resulting in a feature vector $\mathbf{z} = \mathbf{L}\mathbf{s}$ of

size $N = N_{\text{chan}} \times d$. In our implementation, we use a Parseval filterbank \mathbf{T}_θ^\top (tight frame) parametrized by an orthogonal matrix of size $N_{\text{chan}} \times N_{\text{chan}}$, as described in [55]. We also found it beneficial to force all the active regularization filters to have zero mean. This constraint is imposed within our orthogonal parametrization by setting the first convolution mask to be proportional to $\mathbf{1}$, effectively creating a moving average filter.

To learn the regularizer $\mathbf{s} \mapsto \|\mathbf{\Lambda} \mathbf{T}_\theta^\top \mathbf{s}\|_{\ell_1}$ that best represents a given class of signals/images, we follow the strategy of [37] and consider a basic denoising task with $\mathbf{H} = \mathbf{I}$ where the signal is corrupted by additive white Gaussian noise. To adjust the underlying model such as to achieve the best denoising on a representative set of images, we unroll the recurrent neural network in Algorithm 1 and/or use deep equilibrium [56] to learn the model parameters $(\mathbf{\Lambda}, \theta)$.

For the purpose of experimentation, we considered the more general family of optimization problems

$$S_{\text{IV}} = \arg \min_{\mathbf{s} \in \mathbb{R}^d} \frac{1}{2} \|\mathbf{y} - \mathbf{H}\mathbf{s}\|_2^2 + \langle \mathbf{1}, \Phi(\mathbf{T}_\theta^\top \mathbf{s}) \rangle \quad (38)$$

$$= \left\{ \tilde{\mathbf{s}} = \mathbf{T}_\theta \tilde{\mathbf{z}} : \tilde{\mathbf{z}} \in \arg \min_{\mathbf{z} \in \mathbb{R}^N} \frac{1}{2} \|\mathbf{y} - \mathbf{H}\mathbf{T}_\theta \mathbf{z}\|_2^2 + i_{\mathbf{T}_\theta^\top}(\mathbf{z}) + \langle \mathbf{1}, \Phi(\mathbf{z}) \rangle \right\} \quad (39)$$

where $\Phi = (\phi_n) : \mathbb{R}^N \rightarrow \mathbb{R}^N$ is a generic (pointwise) potential with convex component functions $\phi_n : \mathbb{R} \rightarrow \mathbb{R}_{\geq 0}$. Our implementation is based on the equivalent analysis-by-synthesis formulation (39), which decouples the effect of the filters from the nonlinearities induced by Φ . The corresponding regularizer is

$$g(\mathbf{z}) = \langle \mathbf{1}, \Phi(\mathbf{z}) \rangle = \sum_{n=1}^N \phi_n(z_n), \quad (40)$$

which represents the most general separable form of potential. Equation (37) is recovered by setting $\phi_n(z) = \lambda_n |z|$. Here, we also consider the option of learning the ϕ_n using the framework described in [57], which yields an architecture that offers greater expressivity than (37).

Since (39) is the sum of three functionals whose gradient and/or individual proximal maps are easy to compute, it can be minimized efficiently using proximal splitting methods [58]. For our experiments, we adopted the Douglas-Ratchford splitting [59, 60], which resulted in the application-specific implementation summarized in Algorithm 1.

Besides the gradient of the data term, the key components for Algorithm 1 are the proximal maps for: (i) the barrier functional $i_{\mathbf{T}_\theta^\top}(\mathbf{z})$, and (ii)

Algorithm 1 Douglas Ratchford splitting algorithm (DRS) for the resolution of inverse problem with (38) when the potential Φ is separable with known (or trainable) proximal operator prox_{Φ} .

Input: The data vector $\mathbf{y} \in \mathbb{R}^M$, the proximal operator of the potential Φ , the tight frame \mathbf{T}_{θ} , and the step size τ .

Initialization:

$$\mathbf{z}^{(0)} = \mathbf{T}_{\theta}^{\top} \mathbf{H}^{\top} \mathbf{y} \quad (\text{backprojection})$$

Main loop:

for $n = 0, 1, 2, \dots$ **do**

$$\mathbf{z}^{(n+\frac{1}{2})} = \text{prox}_{\tau\Phi} \left(\mathbf{z}^{(n)} - \tau \mathbf{T}_{\theta}^{\top} \mathbf{H}^{\top} (\mathbf{H} \mathbf{T}_{\theta} \mathbf{z}^{(n)} - \mathbf{y}) \right)$$

$$\mathbf{z}^{(n+1)} = \mathbf{T}_{\theta}^{\top} \mathbf{T}_{\theta} \left(2\mathbf{z}^{(n+\frac{1}{2})} - \mathbf{z}^{(n)} \right) + \mathbf{z}^{(n)} - \mathbf{z}^{(n+\frac{1}{2})}$$

end for

Output: $\tilde{\mathbf{s}} = \mathbf{T}_{\theta} \mathbf{z}^{(n)}$ as solution of (38).

the separable regularizer g . The proximal operator of the first corresponds to the projection operator $\mathbf{T}_{\theta}^{\top} \mathbf{T}_{\theta} : \mathbb{R}^N \rightarrow \text{Ran}(\mathbf{T}_{\theta}^{\top})$, which is also used in (36) to indicate the range constraint. The proximal operator for $\|\mathbf{\Lambda} \mathbf{z}\|_{\ell_1}$ is the soft-threshold with parameter $\mathbf{\Lambda}$. The proximal operator for the more general regularizer (40) is separable as well, and given by $\text{prox}_g = (\text{prox}_{\phi_n})$ where each component is defined by

$$\text{prox}_{\phi_n}(x) = \arg \min_{z \in \mathbb{R}} \frac{1}{2}(x - z)^2 + \phi_n(z). \quad (41)$$

These functions must be monotone and firmly non-expansive [36], and can be represented and learned effectively using linear splines, as proposed in [57].

For completeness, and to establish a connection with the best-performing FoE models [37], we also implemented a variant of the reconstruction scheme (Algorithm 2) for differentiable potentials Φ . This variant makes use of the gradient $\nabla \Phi_{\mathbf{z}} = (\phi'_n)$, which can likewise be learned and parameterized using linear splines, as described in [57].

5.5 Experimental results

For validation purposes, we applied our framework to the denoising of natural images and to the reconstruction of magnetic resonance data.

Algorithm 2 Accelerated proximal gradient descent algorithm (APGD) for the resolution of inverse problem (38) when the potential Φ is separable with trainable gradient $\phi = (\phi'_n)$.

Input: The data vector $\mathbf{y} \in \mathbb{R}^M$, the channel-wise derivatives $\varphi = (\phi'_n)$ of the potential functions $\Phi = (\phi_n)$, the tight frame \mathbf{T}_θ , and the step size τ .

Initialization:

$$\mathbf{z}^{(0)} = \mathbf{T}_\theta^\top \mathbf{H}^\top \mathbf{y} \quad (\text{backprojection})$$

Main loop:

for $n = 0, 1, 2, \dots$ **do**

$$\mathbf{z}^{(n+\frac{1}{2})} = \mathbf{z}^{(n)} - \tau (\mathbf{T}_\theta^\top \mathbf{H}^\top (\mathbf{H} \mathbf{T}_\theta \mathbf{z}^{(n)} - \mathbf{y}) + \varphi(\mathbf{z}^{(n)}))$$

$$\mathbf{z}^{(n+1)} = \mathbf{T}_\theta^\top \mathbf{T}_\theta \mathbf{z}^{(n+\frac{1}{2})}$$

end for

Output: $\tilde{\mathbf{s}} = \mathbf{T}_\theta \mathbf{z}^{(n)}$ as solution of (38).

5.5.1 Training

The training was performed on a basic denoising task and is common to both scenarios. The dataset consists of 238400 patches of size (40×40) taken from the BSD500 image dataset [61]. All noise-free images $\mathbf{s} \in \mathbb{R}^d$ are normalized to take values in $[0, 1]$. They were then corrupted with additive Gaussian noise of standard deviation σ to yield the data $\mathbf{y} \in \mathbb{R}^d$.

Our convex denoisers come in three variants: The first, denoted by $\mathbf{f}_{\theta, \Lambda}$, is specified by (37) with $\mathbf{H} = \mathbf{I}$. The second and third are both specified by (39) with $\mathbf{H} = \mathbf{I}$, but differ in the training strategy applied to Φ ; namely, proximal (Algorithm 1) versus gradient-based (Algorithm 2). Since Φ is trainable through its proximity operator, the second architecture is *a priori* more expressive than the first, which is restricted to polyhedral regularization, in accordance with the theory. All denoisers use Parseval filterbanks of size $W \times W$ as regularization operators, with a total number of channel $N_{\text{chan}} = W^2$. These filters are parametrized by an orthogonal matrix $\mathbf{U} \in \mathbb{R}^{N_{\text{chan}} \times N_{\text{chan}}}$. They are trained in PyTorch for the regression task $\mathbf{f}_{\theta, \Lambda}(\mathbf{y}) \approx \mathbf{s}$. During training, the algorithm was run until the relative difference of the iterates fell below $1e-4$. Gradients were estimated via the deep equilibrium framework using the Broyden algorithm with 25 iterates.

Filter Size	3×1	3×3	5×5	7×7	9×9
Total Variation	27.48				
Weighted ℓ_1 (polyhedral norm)		27.86	27.98	28.01	28.03
Learned Prox		27.80	27.98	28.02	28.04
Learned Gradient		27.79	27.95	27.99	28.01

Table 1: PSNR on BSD68 with noise level $\sigma = 25/255$.

5.5.2 Denoising results

The denoising performance on the BSD68 test set is reported in Table 1 for $\sigma = 25/255$. All trained denoisers outperform total variation (TV) denoising, which is included as a baseline. We observe that their performance improves with the number of regularization channels, up to a point where it saturates. Remarkably, the weighted ℓ_1 scheme performs on par with “Learned Prox,” despite the latter having significantly more degrees of freedom and the capacity to learn arbitrary pointwise proximal nonlinearities. Even more striking is the fact that “Learned Prox” converged to nonlinearities that closely resemble soft-threshold functions, as shown in Figure 3. Another general trend is that the learned weight λ_1 for the first channel (corresponding to the moving average) was consistently close to zero, effectively preserving the signal’s lowpass content—see identity-like graph on upper left in Figure 3.

We attribute the slightly lower performance of “Learned Gradient” to its difficulty to learn a polyhedral norm which originates from a potential that is non-differentiable at the origin—an observation that provides additional supports for our universality result.

5.5.3 MRI Reconstruction

For the MRI reconstruction experiments, we used Parseval filters of size 7×7 and followed the same protocol as in [55], with measurement noise of standard deviation 0.1. We investigated three Fourier-domain sampling schemes: (a) random; (b) radial; and (c) (semi-)Cartesian with non-uniform sampling along the horizontal direction—each corresponding to a specific system matrix \mathbf{H} . The reconstruction algorithm was run until the relative difference between successive iterates dropped below 10^{-5} .

The reconstruction performance across the different acquisition protocols and regularization strategies is summarized in Table 2 for two representa-

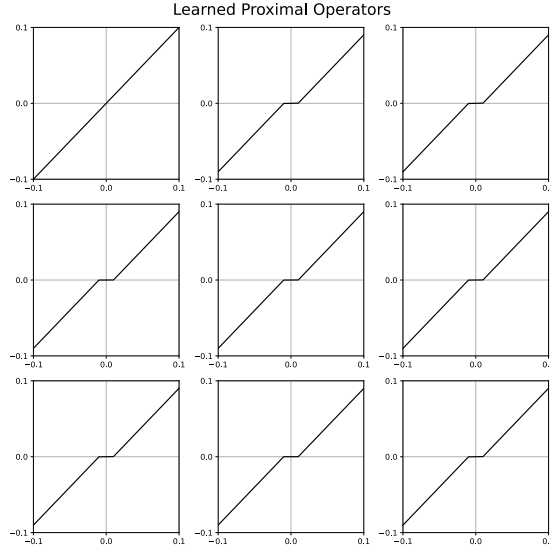


Figure 3: Learned proximal nonlinearities in the $3 \times 3 = 9$ channel scenario.

Subsampling mask Image type	Random		Radial		Cartesian	
	Brain	Bust	Brain	Bust	Brain	Bust
Zero-filling	23.18	24.90	22.57	23.51	20.85	22.34
TV	26.49	28.40	25.71	27.84	22.85	25.57
Weighted ℓ_1	27.48	29.07	26.69	28.53	23.13	25.83
Learned Prox	27.48	29.07	26.70	28.56	23.14	25.84
Learned Grad	27.47	29.05	26.70	28.54	23.12	25.81

Table 2: PSNR values for MRI reconstruction.

tive scans (brain and bust). The overall trend mirrors that observed in the denoising experiments: notably, that our learned polyhedral regularizer performs on par with the two alternative schemes.

The results for the Brain dataset with radial Fourier sampling are shown in Figures 4. In the lower panel, the zero-filled reconstruction exhibits noticeable overlaid textured noise. This reconstruction noise is substantially reduced using total variation (TV)—a method commonly employed for this purpose—and even further suppressed by the three learned regularizers, all of which produce visually similar outputs.

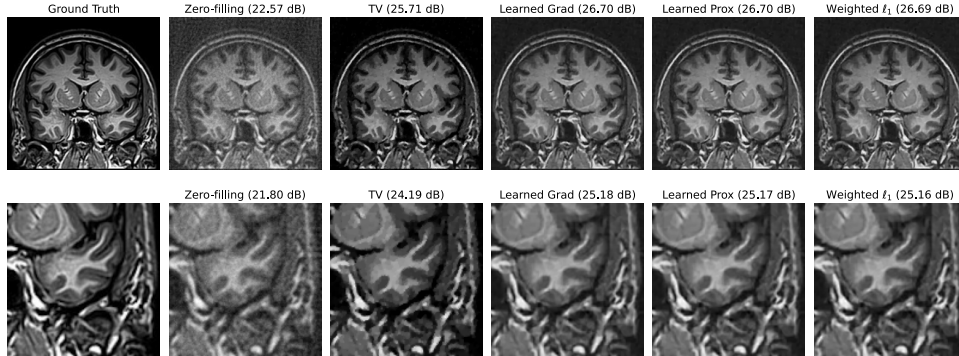


Figure 4: Comparison of ground truth, zero-fill/backprojection $\mathbf{H}^T \mathbf{y}$, and four variational reconstructions of the brain image from radially sampled Fourier data. Lower panel: zoom of a region of interest. The SNR is evaluated with respect to the groundtruth.

5.6 Discussion

Our experiments demonstrate that the weighted- ℓ_1 algorithm matches the performance of state-of-the-art ML frameworks for convex image reconstruction, while requiring significantly fewer parameters and reduced computational resources.

That said, there remains room for improvement, as the architecture used in our experiments only partially exploits the degrees of freedom offered by the polyhedral framework. This limitation arises because of: (i) our use of Parseval filterbanks, rather than general convolutional operators, to simplify training; and (ii) the adoption of an analysis-by-synthesis formulation, which serves only as a proxy for the universal dictionary-based architecture established by our theory.

Further research is needed to develop an architecture that is both machine-learning friendly and universal in the sense described in this work. Such an architecture would help delineate the ultimate capabilities of convex regularization.

Appendix A: (Semi)Norms and Banach Duality

Definition 6 (Norms and seminorms). *A seminorm p on a vector space \mathcal{X} is a real-valued functional $\mathcal{X} \rightarrow \mathbb{R}_{\geq 0}$ that, for all $x \in \mathcal{X}$, satisfies the following properties :*

- *Homogeneity: $|\alpha|p(x) = p(\alpha x)$ for all $\alpha \in \mathbb{R}$ (or \mathbb{C}).*
- *Subadditivity (or triangle inequality): $p(x + y) \leq p(x) + p(y)$ for all $x, y \in \mathcal{X}$.*

If, in addition, $p(x) = 0 \Leftrightarrow x = 0$ (positive-definiteness), then p is called norm and is commonly denoted by $\|\cdot\| = p(\cdot)$.

A normed space is a vector space equipped with a norm—the generic form being $(\mathcal{X}, \|\cdot\|_{\mathcal{X}})$. The latter is a Banach space whenever it is complete; that is, when every Cauchy sequence in $(\mathcal{X}, \|\cdot\|_{\mathcal{X}})$ has a limit in \mathcal{X} .

We denote the (closed) unit ball of a Banach space $\mathcal{X} = (\mathcal{X}, \|\cdot\|_{\mathcal{X}})$ by $B_{\mathcal{X}}$ with

$$B_{\mathcal{X}} = \{x \in \mathcal{X} : \|x\|_{\mathcal{X}} \leq 1\}. \quad (42)$$

The continuous dual of \mathcal{X} is the vector space \mathcal{X}' of continuous linear functionals on \mathcal{X} with generic element $f : x \mapsto \langle f, x \rangle \in \mathbb{R}$. A fundamental property is that $\mathcal{X}' = (\mathcal{X}', \|\cdot\|_{\mathcal{X}'})$ equipped with the dual norm

$$\forall f \in \mathcal{X}' : \quad \|f\|_{\mathcal{X}'} = \sup_{x \in B_{\mathcal{X}}} \langle f, x \rangle. \quad (43)$$

is a Banach space as well [40].

The unit ball $B_{\mathcal{X}}$ is a convex, center-symmetric subset of \mathcal{X} (i.e., a disk) whose rescaled versions specify all Banach neighborhoods of the origin $0 \in \mathcal{X}$. Similar to (43) which makes an explicit connection between $B_{\mathcal{X}}$ and the dual norm, it is possible to relate $B_{\mathcal{X}}$ to the initial norm $\|\cdot\|_{\mathcal{X}} = \mu_{B_{\mathcal{X}}}(\cdot)$ with the help of the Minkowski functional (see Theorem 2).

In finite dimensions, one defines the polar of any subset $B \subset \mathbb{R}^d$ as

$$B^{\circ} = \{\mathbf{y} \in \mathbb{R}^d : \langle \mathbf{y}, \mathbf{x} \rangle \leq 1, \mathbf{x} \in B\} = \{\mathbf{y} \in \mathbb{R}^d : \sup_{\mathbf{x} \in B} \langle \mathbf{y}, \mathbf{x} \rangle \leq 1\}, \quad (44)$$

with the latter necessarily being a closed convex subset of \mathbb{R}^d that contains the origin (see [49]). If $B = B_{\mathcal{X}}$ is the unit ball of the Banach space $\mathcal{X} = (\mathbb{R}^d, \|\cdot\|_{\mathcal{X}})$, then its polar $B_{\mathcal{X}}^{\circ}$ coincides with the unit ball $B_{\mathcal{X}'}$ of the dual space, in conformity with (43). Accordingly, we have that $\mathcal{X}' = (\mathbb{R}^d, \mu_{B_{\mathcal{X}}^{\circ}}(\cdot)) = (\mathbb{R}^d, \|\cdot\|_{\mathcal{X}'})$, as well as $(B_{\mathcal{X}}^{\circ})^{\circ} = B_{\mathcal{X}}$ because \mathcal{X} is reflexive.

Acknowledgments

The research was supported by the European Commission under Grant ERC-2020-AdG FunLearn-101020573.

References

- [1] F. Natterer, *The Mathematics of Computed Tomography*. John Willey & Sons Ltd., 1984.
- [2] Z.-P. Liang and P. C. Lauterbur, *Principles of Magnetic Resonance Imaging: A Signal Processing Perspective*. Wiley-IEEE Press, 2000.
- [3] M. McCann and M. Unser, “Biomedical image reconstruction: From the foundations to deep neural networks,” *Foundations and Trends in Signal Processing*, vol. 13, pp. 280–359, Dec. 2019.
- [4] I. Ekeland and R. Temam, *Convex Analysis and Variational Problems*, vol. 28 of *Classics in Applied Mathematics*. SIAM, 1999.
- [5] S. Boyd and L. Vandenberghe, *Convex Optimization*. Cambridge University Press, 2004.
- [6] S. Foucart and H. Rauhut, *A Mathematical Introduction to Compressive Sensing*. Springer, 2013.
- [7] M. A. T. Figueiredo and R. D. Nowak, “An EM algorithm for wavelet-based image restoration,” *IEEE Transactions on Image Processing*, vol. 12, no. 8, pp. 906–916, 2003.
- [8] P. Combettes and V. Wajs, “Signal recovery by proximal forward-backward splitting,” *Multiscale Modeling & Simulation*, vol. 4, pp. 1168–1200, 2005.
- [9] M. A. Figueiredo, R. D. Nowak, and S. J. Wright, “Gradient projection for sparse reconstruction: Application to compressed sensing and other inverse problems,” *IEEE Journal of Selected Topics in Signal Processing*, vol. 1, no. 4, pp. 586–597, 2007.
- [10] A. Beck and M. Teboulle, “Fast gradient-based algorithms for constrained total variation image denoising and deblurring problems,” *IEEE Transactions on Image Processing*, vol. 18, pp. 2419–2434, Nov. 2009.

- [11] P. del Aguila Pla, S. Neumayer, and M. Unser, “Stability of image-reconstruction algorithms,” *IEEE Transactions on Computational Imaging*, vol. 9, pp. 1–12, 2023.
- [12] D. L. Donoho, “Compressed sensing,” *IEEE Transactions on Information Theory*, vol. 52, no. 4, pp. 1289–1306, 2006.
- [13] E. J. Candès and J. Romberg, “Sparsity and incoherence in compressive sampling,” *Inverse Problems*, vol. 23, no. 3, pp. 969–985, 2007.
- [14] K. H. Jin, M. T. McCann, E. Froustey, and M. Unser, “Deep convolutional neural network for inverse problems in imaging,” *IEEE Transactions on Image Processing*, vol. 26, pp. 4509–4522, Sept. 2017.
- [15] M. McCann, K. Jin, and M. Unser, “Convolutional neural networks for inverse problems in imaging—a review,” *IEEE Signal Processing Magazine*, vol. 34, pp. 85–95, Nov. 2017.
- [16] G. Wang, J. C. Ye, and B. De Man, “Deep learning for tomographic image reconstruction,” *Nature Machine Intelligence*, vol. 2, pp. 737–748, Dec. 2020.
- [17] D. J. Lin, P. M. Johnson, F. Knoll, and Y. W. Lui, “Artificial intelligence for MR image reconstruction: an overview for clinicians,” *Journal of Magnetic Resonance Imaging*, vol. 53, no. 4, pp. 1015–1028, 2021.
- [18] J. C. Ye, Y. C. Eldar, and M. A. Unser, *Deep Learning for Biomedical Image Reconstruction*. Cambridge University Press, 2023.
- [19] V. Antun, F. Renna, C. Poon, B. Adcock, and A. C. Hansen, “On instabilities of deep learning in image reconstruction and the potential costs of AI,” *Proceedings of the National Academy of Sciences*, vol. 117, pp. 30088–30095, May 2020.
- [20] G. Nataraj and R. Otazo, “Model-free deep MRI reconstruction: A robustness study,” in *ISMRM Workshop on Data Sampling and Image*, 2020.
- [21] M. J. Muckley, B. Riemenschneider, A. Radmanesh, S. Kim, G. Jeong, J. Ko, Y. Jun, H. Shin, D. Hwang, M. Mostapha, S. Arberet, D. Nickel, Z. Ramzi, P. Ciuciu, J.-L. Starck, J. Teuwen, D. Karkaloulos, C. Zhang, A. Sriram, Z. Huang, N. Yakubova, Y. W. Lui, and F. Knoll, “Results of

- the 2020 fastMRI challenge for machine learning MR image reconstruction,” *IEEE Transactions on Medical Imaging*, vol. 40, pp. 2306–2317, Sept. 2021.
- [22] K. Hammernik, T. Klatzer, E. Kobler, M. P. Recht, D. K. Sodickson, T. Pock, and F. Knoll, “Learning a variational network for reconstruction of accelerated MRI data,” *Magnetic Resonance in Medicine*, vol. 79, no. 6, pp. 3055–3071, 2018.
- [23] H. K. Aggarwal, M. P. Mani, and M. Jacob, “MoDL: Model-based deep learning architecture for inverse problems,” *IEEE Transactions on Medical Imaging*, vol. 38, no. 2, pp. 394–405, 2019.
- [24] V. Monga, Y. Li, and Y. C. Eldar, “Algorithm unrolling: Interpretable, efficient deep learning for signal and image processing,” *IEEE Signal Processing Magazine*, vol. 38, pp. 18–44, Mar. 2021.
- [25] S. Roth and M. J. Black, “Fields of experts,” *International Journal of Computer Vision*, vol. 82, pp. 205–229, Jan. 2009.
- [26] Y. Chen and T. Pock, “Trainable nonlinear reaction diffusion: A flexible framework for fast and effective image restoration,” *IEEE Transactions on Pattern Analysis and Machine Intelligence*, vol. 39, no. 6, pp. 1256–1272, 2017.
- [27] H. Nguyen, E. Bostan, and M. Unser, “Learning convex regularizers for optimal Bayesian denoising,” *IEEE Transactions on Signal Processing*, vol. 66, pp. 1093–1105, Feb. 2018.
- [28] A. Goujon, S. Neumayer, and M. Unser, “Learning weakly convex regularizers for convergent image-reconstruction algorithms,” *SIAM Journal on Imaging Sciences*, vol. 17, no. 1, pp. 91–115, 2024.
- [29] S. V. Venkatakrishnan, C. A. Bouman, and B. Wohlberg, “Plug-and-play priors for model based reconstruction,” in *2013 IEEE Global Conference on Signal and Information Processing*, pp. 945–948, 2013.
- [30] U. S. Kamilov, C. A. Bouman, G. T. Buzzard, and B. Wohlberg, “Plug-and-play methods for integrating physical and learned models in computational imaging: Theory, algorithms, and applications,” *IEEE Signal Processing Magazine*, vol. 40, pp. 85–97, Jan. 2023.

- [31] E. Ryu, J. Liu, S. Wang, X. Chen, Z. Wang, and W. Yin, “Plug-and-play methods provably converge with properly trained denoisers,” in *International Conference on Machine Learning*, pp. 5546–5557, PMLR, 2019.
- [32] Y. Sun, Z. Wu, X. Xu, B. Wohlberg, and U. S. Kamilov, “Scalable plug-and-play ADMM with convergence guarantees,” *IEEE Transactions on Computational Imaging*, vol. 7, pp. 849–863, 2021.
- [33] D. H. Ye, S. Srivastava, J.-B. Thibault, K. Sauer, and C. Bouman, “Deep residual learning for model-based iterative CT reconstruction using Plug-and-Play framework,” in *IEEE International Conference on Acoustics, Speech and Signal Processing*, pp. 6668–6672, 2018.
- [34] J. Hertrich, S. Neumayer, and G. Steidl, “Convolutional proximal neural networks and Plug-and-Play algorithms,” *Linear Algebra and Its Applications*, vol. 631, pp. 203–234, 2021.
- [35] H. H. Bauschke, S. M. Moffat, and X. Wang, “Firmly nonexpansive mappings and maximally monotone operators: Correspondence and duality,” *Set-Valued and Variational Analysis*, vol. 20, no. 1, pp. 131–153, 2012.
- [36] R. Gribonval and M. Nikolova, “A characterization of proximity operators,” *Journal of Mathematical Imaging and Vision*, vol. 62, pp. 773–789, Mar. 2020.
- [37] A. Goujon, S. Neumayer, P. Bohra, S. Ducotterd, and M. Unser, “A neural-network-based convex regularizer for inverse problems,” *IEEE Transactions on Computational Imaging*, vol. 9, pp. 781–795, 2023.
- [38] R. Rubinstein, A. M. Bruckstein, and M. Elad, “Dictionaries for sparse representation modeling,” *Proceedings of the IEEE*, vol. 98, no. 6, pp. 1045–1057, 2010.
- [39] M. Elad, *Sparse and Redundant Representations. From Theory to Applications in Signal and Image Processing*. Springer, 2010.
- [40] R. E. Megginson, *An Introduction to Banach Space Theory*, vol. 183. Springer Science & Business Media, 2012.
- [41] L. Narici and E. Beckenstein, *Topological Vector Spaces*. No. 296 in Pure and Applied Mathematics, Boca Raton, FL: CRC Press, 2nd ed., 2010.

- [42] P. M. Gruber and P. Kenderov, “Approximation of convex bodies by polytopes,” *Rendiconti del Circolo Matematico di Palermo*, vol. 31, pp. 195–225, June 1982.
- [43] E. M. Bronstein, “Approximation of convex sets by polytopes,” *Journal of Mathematical Sciences*, vol. 153, pp. 727–762, Sept. 2008.
- [44] E. M. Bronshteyn and L. Ivanov, “The approximation of convex sets by polyhedra,” *Siberian Mathematical Journal*, vol. 16, no. 5, pp. 852–853, 1975.
- [45] G. M. Ziegler, *Lectures on Polytopes*, vol. 152. Springer Science & Business Media, 2012.
- [46] V. Klee, “Polyhedral sections of convex bodies,” *Acta Mathematica*, no. 103, pp. 243–267, 1960.
- [47] J. Lindenstrauss, “Notes on Klee’s paper “Polyhedral sections of convex bodies”,” *Israel Journal of Mathematics*, vol. 4, no. 4, pp. 235–242, 1966.
- [48] B. Grünbaum, *Convex Polytopes*. Springer, 2nd ed., 2000.
- [49] A. Brøndsted, *An Introduction to Convex Polytopes*, vol. 90. Springer Science & Business Media, 2012.
- [50] O. Christensen, *An Introduction to Frames and Riesz Bases*. Birkhauser, 2003.
- [51] Y. Chen, T. Pock, and H. Bischof, “Learning ℓ_1 -based analysis and synthesis sparsity priors using bi-level optimization,” Jan. 2014.
- [52] D. Carrera, G. Boracchi, A. Foi, and B. Wohlberg, “Sparse overcomplete denoising: Aggregation versus global optimization,” *IEEE Signal Processing Letters*, vol. 24, pp. 1468–1472, Oct. 2017.
- [53] D. Simon and M. Elad, “Rethinking the CSC Model for Natural Images,” in *Advances in Neural Information Processing Systems*, vol. 32, Curran Associates, Inc., 2019.
- [54] G. E. Shilov, *Linear algebra*. Dover Publications, Inc., 1977.
- [55] M. Unser and S. Ducotterd, “Parseval convolution operators and neural networks,” *arXiv preprint arXiv:2408.09981 [eess.SP]*, 2024.

- [56] D. Gilton, G. Ongie, and R. Willett, “Deep Equilibrium Architectures for Inverse Problems in Imaging,” *IEEE Transactions on Computational Imaging*, vol. 7, pp. 1123–1133, 2021. Conference Name: IEEE Transactions on Computational Imaging.
- [57] M. Unser, A. Goujon, and S. Ducotterd, “Controlled learning of pointwise nonlinearities in neural-network-like architectures,” *Applied and Computational Harmonic Analysis*, in press.
- [58] L. Condat, D. Kitahara, A. Contreras, and A. Hirabayashi, “Proximal splitting algorithms for convex optimization: A tour of recent advances, with new twists,” *SIAM Review*, vol. 65, pp. 375–435, May 2023.
- [59] L. M. Briceno-Arias, “Forward-Douglas/Rachford splitting and forward-partial inverse method for solving monotone inclusions,” *Optimization*, vol. 64, pp. 1239–1261, Dec. 2013.
- [60] H. Raguet, “A note on the forward-Douglas/Rachford splitting for monotone inclusion and convex optimization,” *Optimization Letters*, vol. 13, pp. 717–740, May 2018.
- [61] P. Arbeláez, M. Maire, C. Fowlkes, and J. Malik, “Contour detection and hierarchical image segmentation,” *IEEE Transactions on Pattern Analysis and Machine Intelligence*, vol. 33, no. 5, pp. 898–916, 2011.